1 Mammalian bioturbation amplifies rates of both, hillslope sediment erosion and accumulation,

2 in coastal Chile

3 *Paulina Grigusova[1], Annegret Larsen[2], Roland Brandl[3], Camilo del Río[4,5], Nina Farwig[6], Diana Kraus[6],*

4 *Leandro Paulino[7], Patricio Pliscoff[4,8,9], Jörg Bendix[1]*

7 [1] Laboratory for Climatology and Remote Sensing, Department of Geography, University of Marburg,

8 35037 Marburg, Germany; paulina.grigusova@staff.uni-marburg.de (P.G.); bendix@geo.uni-

9 marburg.de (J.B.)

10 [2] Soil Geography and Landscape, Department of Environmental Sciences,

11 Wageningen University & Research, 6700 AA Wageningen, The Netherlands; annegret.larsen@wur.nl

12 [3] Animal Ecology, Department of Biology, University of Marburg, 35032 Marburg, Germany;

13 brandlr@biologie.uni-marburg.de

14 [4] Facultad de Historia, Geografía y Ciencia Política, Instituto de Geografía, Pontificia Universidad Católica

15 de Chile, 782-0436 Santiago, Chile; cdelriol@uc.cl

16 [5] Centro UC Desierto de Atacama, Pontificia Universidad Católica de Chile, 782-0436 Santiago, Chile

17 [6] Conservation Ecology, Department of Biology, University of Marburg, 35047 Marburg, Germany;

18 diana.kraus@biologie.uni-marburg.de (D.K.); nina.farwig@biologie.uni-marburg.de (N.F.)

19 [7] Facultad de Agronomía, Universidad de Concepción, 3780000 Chillán, Chile; lpaulino@udec.cl

20 [8] Facultad de Ciencias Biológicas, Departamento de Ecología, Pontificia Universidad Católica de Chile,

21 8331150 Santiago, Chile; pliscoff@uc.cl

22 [9] Center of Applied Ecology and Sustainability (CAPES), Pontificia Universidad Católica de Chile,

23 8331150 Santiago, Chile; pliscoff@uc.cl

25 Corresponding author:

26 Paulina Grigusova

27 paulina.grigusova@staff.uni-marburg.de

42 **Abstract**

43 Soil bioturbation activity affects soil texture, bulk density, soil water content and redistribution of

44 nutrients. All of these parameters influences sediment redistribution, which shapes the earth surface.

45 Hence it is important to include bioturbation into erosion models. However, up to present, the inclusion

46 of bioturbation into erosion models was limited. This is because to realistically include bioturbation into

47 the modelling, the interplay between bioturbation, sediment redistribution and environmental parameters

48 is not understood.

49 Here, we included bioturbation into a soil erosion model and interpreted the impacts of bioturbation on

50 sediment redistribution. To do this, we measured the needed soil properties and location of burrows

51 created by bioturbating animals in four research sites located along the Chilean climate gradient. Then,

52 we parametrized a semi-empirical erosion model by applying machine learning algorithms to upscale

53 soil properties and burrow distribution. We ran the model for a time period of 6 years under two

54 conditions: With and without bioturbation. We validated the model using several sediment fences in the

55 field. We estimated the modelled sediment redistribution and surface runoff in all climate zones. Lastly,

56 we identified environmental parameters determining the positive or negative impact of bioturbation on

57 sediment redistribution.

58 We found that the model with integrated bioturbation performed much better (R^2 = 0.71, RMSE = 0.63)

59 than the model without integrated bioturbation (R^2 = 0.17, RMSE = 1.18), meaning that model runs which

60 considered bioturbation predicted the sediment redistribution more realistically. Furthermore,

61 bioturbation increased sediment redistribution in all but the humid climate zone, especially in the

62 Mediterranean zone. The quantity of sediment redistributed due to bioturbation was reliant on an

63 interplay between elevation, slope, surface roughness and sink connectivity. Overall, bioturbation

64 enhances sediment erosion in areas where more erosion is expected, and enhances sediment

65 accumulation in areas which are more prone to accumulate sediment. In other words, considering

66 bioturbation when studying earth surface evolution means an amplification of existing tendencies in

67 sediment redistribution, and leads to a faster hillslope relief equalisation.

68
69
70
71
72
73
74
75
76
77
78
79
80
81
82

1. Introduction

83

84   Bioturbation was shown to shape the land surface (Hazelhoff et al., 1981; Istanbulluoglu, 2005; Taylor

85   et al., 2019; Tucker and Hancock, 2010; Whitesides and Butler, 2016; Wilkinson et al., 2009; Corenblit

86   et al., 2021) by influencing surface microtopography (Reichman and Seabloom, 2002; Kinlaw and

87   Grasmueck, 2012; Debruyn and Conacher, 1994), and soil properties such as soil porosity, permeability

88   and infiltration (Reichman and Seabloom, 2002; Yair, 1995; Hancock and Lowry, 2021; Ridd, 1996; Hall

89   et al., 1999; Coombes, 2016; Larsen et al., 2021). Cumulatively, these modifications lead to changes in

90   sediment redistribution (Gabet et al., 2003; Nkem et al., 2000; Wilkinson et al., 2009) and hence have

91   the potential to affect surface topography and nutrient redistribution on large spatial and temporal scale.

92   To quantify these effects, the shared role of climate, landscape characteristics and burrowing dynamics

93   on sediment redistribution needs to be understood.

94   On a local scale, currently used field methods to monitor sediment redistribution under real-life condition

95   are mainly erosion pins, splash boards, or rainfall simulators (Imeson and Kwaad, 1976; Wei et al., 2007;

96   Le Hir et al., 2007; Li et al., 2019a; Li et al., 2019b; Li et al., 2018; Voiculescu et al., 2019; Chen et al.,

97   2021; Übernickel et al., 2021a). The monitoring of box experiments yields a high spatio-temporal

98   resolution, and can also be linked with mathematical equations, such as random walks (Boudreau, 1986;

99   Wheatcroft et al., 1990), stochastic differential equations (Boudreau, 1989; Milstead et al., 2007), finite

100 difference mass balancing (Soetaert et al., 1996; François et al., 1997) or Markov chain theory (Jumars

101 et al., 1981; Foster, 1985; Trauth, 1998; Shull, 2001) to describe sediment redistribution. Another

102 approach offer raster-based soil erosion and landscape evolution models which integrate co-

103 dependencies between bioturbation relevant environmental parameters (Black and Montgomery, 1991;

104 Meysman et al., 2003; Yoo et al., 2005; Schiffers et al., 2011). Most common soil erosion models are

105 empirical (Wischmeier and Smith, 1978; Williams, 1975; Renard et al., 1991), process-based (Morgan

106 et al., 1998; ROO et al., 1996; Nearing et al., 1989; Beasley et al., 1980), or semi-empirical models, the

107 latter of which are a combination of both (Morgan et al., 1984; BEVEN and KIRKBY, 1979). Empirical

108 models are limited to one study site, but they provide highly accurate predictions at low computational

109 costs, as they are based on simple mathematical equations. In contrast, process-based models require

110 an intensive parametrisation and calibration process, however, once calibrated, they can be applied to

111 almost any site (Lal, 2001; Merritt et al., 2003). Semi-empirical models combine semi-empirical

112 equations with a physical basis and thus include the advantages of the both model types (Morgan et al.,

113 1984; Morgan, 2001; Morgan and Duzant, 2008; Devia et al., 2015; Lilhare et al., 2015).

114 Previously used methods have, however, several limitations when studying bioturbation. Field

115 measurements likely lead to an underestimation of sediment fluxes, as they are one-time or seasonal

116 measurements, and thus do not capture the continuous excavation of the sediment by the animal

117 (Grigusova et al., 2022) at a high temporal resolution. Box experiments and from them derived

118 mathematical equations describe bioturbation as an isolated process and ignore surrounding

119 environmental parameters (such as climate or vegetation). Most erosion or landscape evolution models

120 do not yet implement impacts of bioturbators on water and sediment fluxes (Brosens et al., 2020;

121 Anderson et al., 2019; Braun et al., 2016; Cohen et al., 2015; Cohen et al., 2010; Carretier et al., 2014;

122 Welivitiya et al., 2019). Models which include bioturbation as an input factor still have large limitations.

123 They predict landscape evolution on a millennial scale, but ignore processes acting on a daily basis.

124   This rather large spatio-temporal scale also means an omission of the natural variability in burrow sizes
125   and densities, climate zones and seasonality (Temme and Vanwalleghem, 2016; Vanwalleghem et al.,
126   2013; Yoo and Mudd, 2008; Pelletier et al., 2013). The most significant limitation is, however, that in all
127   models bioturbation is hard-coded to have predefined effects on the environment: (i) soil erosion is
128   proportionally increasing with increasing bioturbation, (ii) vertical soil mixing rates are uniform, and (iii)
129   bioturbation is positively linked with vegetation cover. Thus, none of these models consider that the
130   interaction of bioturbation with environmental parameters and the effect on sediment redistribution may
131   not be uniform but context dependent. However, the field measurements showed both, positive
132   (Hazelhoff et al., 1981; Black and Montgomery, 1991; Chen et al., 2021) and negative impact of
133   bioturbation on erosion (Imeson and Kwaad, 1976; Hakonson, 1999). Also, previous field based studies
134   observed an increased bioturbation activity with higher (Milstead et al., 2007; Meserve, 1981; Tews et
135   al., 2004; Wu et al., 2021; Ferro and Barquez, 2009), but also with lower vegetation cover (Simonetti,
136   1989; Zhang et al., 2020; Zhang et al., 2019; Qin et al., 2021). Furthermore, soil mixing rates are not
137   homogenous throughout the year but depend on the animal phenological cycles (Eccard and Herde,
138   2013; Jimenez et al., 1992; Katzman et al., 2018; Malizia, 1998; Morgan and Duzant, 2008; Monteverde
139   and Piudo, 2011; Gray et al., 2020; Yu et al., 2017).
140   To improve this, bioturbation has to be included into erosion models at a high spatial and temporal
141   resolution under real-life conditions across several climate zones. A suitable model which can be
142   extended to include continuous bioturbating activity is the semi-empirical Morgan – Morgan – Finney
143   soil erosion model (Morgan et al., 1984; Morgan, 2001). This model was successfully tested in several
144   climate zones and land use types, such as Mediterranean sites (Jong et al., 1999), rainfed agrosystems,
145   fields and pastures (López-Vicente et al., 2008), East-African Highlands (Vigiak et al., 2005) or humid
146   forests (Vieira et al., 2014). One of the recently developed improvements of this model is the Daily
147   Morgan – Morgan – Finney model (DMMF), which introduces subsurface flow, vegetation structures
148   (type, size, height, root depth), and enables modelling at a high spatial (0.5 m) and temporal (daily)
149   resolution (Choi et al., 2017). These improvements yield the potential to integrate the bioturbation into
150   the model, as the burrowing activity is not constant and depends on vegetation structure (Tews et al.,
151   2004; Ferro and Barquez, 2009).
152   To study the interplay between bioturbation, environmental parameters and sediment redistribution
153   along a climate gradient, we (i) include bioturbation into a semi-empirical soil erosion model (DMMF) at
154   a high temporal and spatial resolution. We specifically not presuppose a homogenous relationship
155   between bioturbation, sediment transport and vegetation cover. Based on (i), we (ii) identify
156   environmental parameters which determine if the bioturbation enhances sediment erosion or sediment
157   accumulation. In order to do this, we included bioturbation into the DMMF while considering (i) variable
158   co-dependency between bioturbation and vegetation type, density and height; (ii) various burrow sizes
159   and burrow densities, (iii) variable soil mixing rates due to continuous reconstruction of the burrow by
160   the animal depending on season and (iv) variable influence of bioturbation on litter and coarse grain
161   size. Furthermore, we set up generalized additive models to unveil significant environmental parameters
162   that determine the impact of bioturbation on sediment redistribution. Lastly, we analyse how the impact
163   of bioturbation on sediment redistribution depends on the burrow structure, climate, topography and

164   surrounding vegetation. Our study shows the importance of including bioturbation into erosion modelling

165   and the interplay between bioturbation, environmental parameters and sediment redistribution.

166

167   **2. Study area**

168   Our study was performed along a climate and vegetation gradient in Chile (Übernickel et al., 2021b),

169   comprising four study sites in the Chilean Coastal Cordillera: Pan de Azúcar (PdA) National Park (NP),

170   Santa Gracia (SG), La Campana (LC) NP, and Nahuelbuta (NA) NP (Fig. 1). PdA NP is located in the

171   arid zone in a fog-laden environment in the southern part of the Atacama Desert, with almost no rainfall.

172   The vegetation cover is less than 5 % and dominated by small desert shrubs, several types of cacti and

173   biocrusts (Lehnert et al., 2018). SG is a natural reserve located in the semi-arid zone near La Serena,

174   which is dominated by goat grazing. The vegetation consists of shrubs and cacti, covering up to 40 %

175   of the study area. LC NP is part of the Mediterranean-type climate zone in the Valparaiso Region and is

176   also affected by cattle. The study site is dominated by an evergreen sclerophyllous forest with endemic

177   palms. The canopy reaches a height of up to 9 m, and the understory consists of deciduous shrubs and

178   herbs. NA is located in the humid-temperate zone and characterized by a dense evergreen *Araucaria*

179   forest comprising broadleaved trees with heights of up to 14 m. The ground is covered by bamboo,

180   shrubs, and herbs (Bernhard et al., 2018; Oeser et al., 2018). The most common bioturbating vertebrate

181   animal species recorded within these sites are carnivores of the family Canidae (*Lycalopex culpaeus*,

182   *Lycalopex griseus*) as well as rodents of the families Abrocomidae (*Abrocoma bennetti)*, Chnichillidae

183   (*Lagidium viscacia)*, Cricetidae (*Abrothrix andinus, Phyllotis xanthopygus, Phyllotis limatus, Phyllotis*

184   *darwini*) and Octogontidae (Cerqueira, 1985; Jimenez et al., 1992; Übernickel et al., 2021a).

185
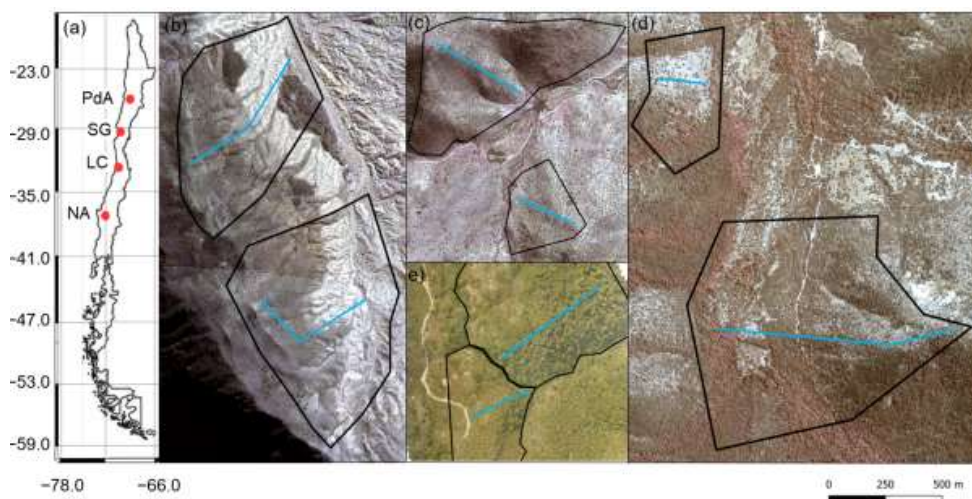
186

187   **Figure 1.** Study area and study sites. Black lines outline the catchments. Along the blue lines, the in situ

188   data (mound locations, soil samples, vegetation mapping) were collected. (a) Position of the study sites

189   along the climate gradient. PdA = Pan de Azúcar, SG = Santa Gracia, LC = La Campana, NA =

190   Nahuelbuta; Positions of plots in (b) PdA; (c) SG; (d) LC; and (e) NA. The background image is an RGB-

191   composite calculated from WorldView-2 satellite imagery. Images were obtained with single license from

192   GAF AG.

193

194   **3. Methodology**

195   We combined semi-empirical soil erosion modelling with in-situ measurements, remote sensing data

196   and machine learning methods (Fig. 2). Along 8 catchments within 4 climate zones we mapped locations

197   of burrows, estimated the vegetation cover and extracted soil samples. We analyzed the soil samples

198   in the laboratory. Then we used remote sensing datasets and machine learning to upscale burrow

199   distribution, vegetation cover and soil properties into the catchments. The catchment-wide predictions,

200   the topographical information retrieved from LiDAR data (Kügler et al., 2022) and the climate information

201   retrieved from climate stations were the input parameters for our soil erosion model. We ran the model

202   with and without bioturbation. We included the bioturbation into the model by adjusting the input

203   parameters at the predicted burrow locations, by including the continuous burrowing activity and soil

204   mixing (Grigusova et al., 2021), and the seasonality (Kraus et al., 2022).and the animal phenological

205   cycle as found in (Jimenez et al., 1992). The models were validated using self-constructed sediment

206   traps. We studied the modeled surface runoff and sediment redistribution. Lastly, we analyzed if and

207   how the impact of bioturbation on sediment redistribution depends on environmental parameters

208   (topography, landscape connectivity and vegetation).

209

210
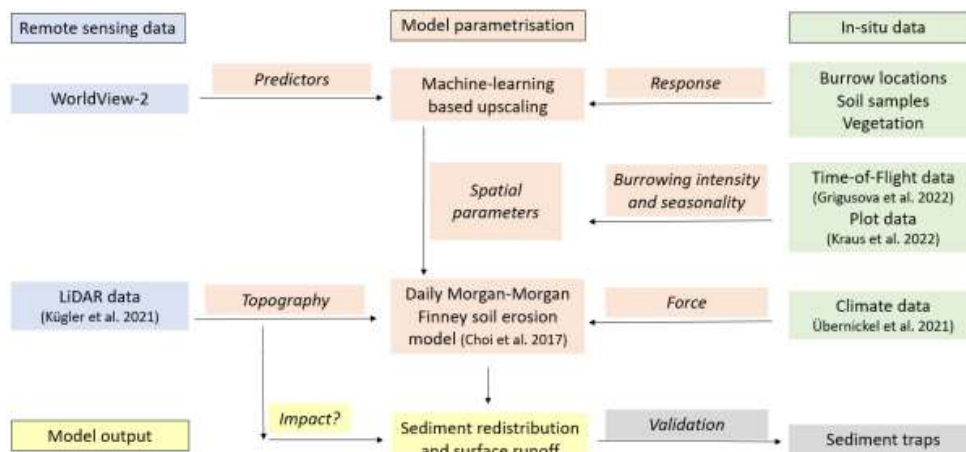
211

212   **Figure 2.** Flow chart of our study. Green color indicates in-situ input data, blue indicates remote sensing

213   input data. Red indicates Model parametrization. Yellow indicates model output and analysis. Grey

214   indicates model validation.

215

216   **3.1 In-situ data**

217   The study set-up consisted of eight hillside catchments: one north-facing and one south-facing hillside

218   catchment per study site. We defined a line with a width of one meter from the top to the base of each

219 hillside catchment (see blue line, Fig. 1). We subdivided the track into tiles of 1 m². We saved the GPS
220 information of each tile.

221 Within each tile of the line, we mapped burrow presence, land cover and extracted soil samples. A
222 burrow consisted of an entrance and a mound (Fig. 3a). Each 1 m² tile with a burrow was described as
223 a presence data point, tiles without a burrow as absence data points. We noted the size of the burrow,
224 vegetation cover and land cover types (bare soil, herbs, shrubs, trees) within the tile. We extracted 162
225 soil samples from soil without a mound at a depth of 10 cm. Additionally, we took a photo of the surface
226 every second tile along the track.

227 To validate the model output, we set up sediment traps (Fig. 3b), with six traps per site, two of which
228 were located at the catchment base and four were located on two random positions within the catchment.
229 The sediment traps consisted of geotextile vertically attached to wooden poles for stability. The traps
230 had a length of 2 m – 5 m, a width of ~1.5 m and a height of ~1 m. 1.5 m of geotextile was laid down at
231 the surface uphill the wooden poles to enable the collection of sediment. The sediment accumulated
232 within the traps was collected after 1 year and its mass [cm³] and dry weight [kg] were estimated.

233 Climate information was retrieved from climate stations located adjacent to the catchments which
234 provide climate data in 5 minute intervals (Übernickel et al. 2021). To force the model on an hourly basis,
235 hourly air temperature, precipitation total and intensity, wind speed, wind direction and humidity was
236 calculated for the study period from 1st April 2016 to 1st December 2021. Evapotranspiration was
237 estimated by the Penman-Monteith equation (Penman, 1948).

238
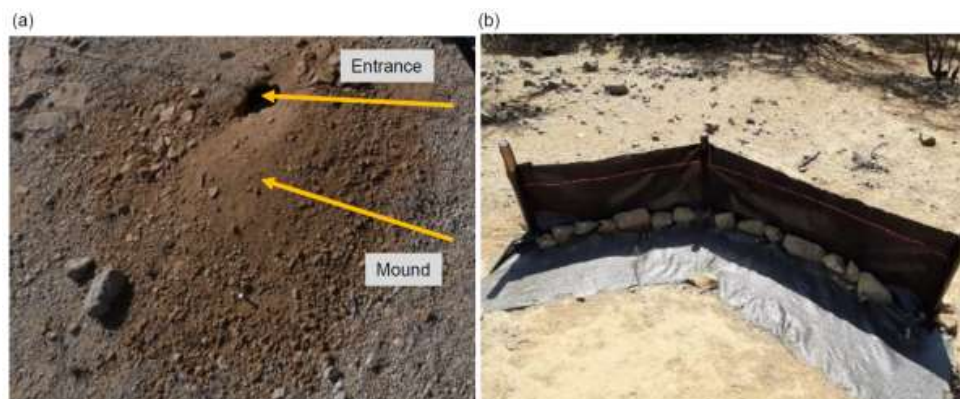
239

240 **Figure 3.** In-situ constructions. (a) Example of a burrow consisting of burrow entrance and mound. (b)
241 Fence construction used for the collection of eroded sediment to validate the model. Both photos by
242 Paulina Grigusova.

243

244 **3.2 Estimation of soil properties**

245 We estimated several soil properties from the soil samples and photos collected in-situ ((Grigusova et
246 al., 2022). We estimated above-ground skeleton and debris from the photos taken every second tile.
247 For this, the photos were firstly classified into 5 classes. The classification was unsupervised using k-
248 means (Fig. A1). Then we calculated the ratio of pixels classified as skeleton and / or debris to the
249 overall amount of all pixels to determine the amount of both parameters in percent.

250   In the lab, we estimated soil water content, bulk density, soil particle density, soil texture (sand, silt, clay,

251   coarse / middle / fine sand, coarse / middle / fine silt), soil skeleton, organic matter and organic carbon.

252   Gravimetric soil water content [%] (GSWC) described the mass of water within the soil sample and was

253   estimated as in Eq (1):

254    $GSWC = \frac{(Sm - Sd)}{Sd} * 100$,   (1)

255   where Sm [g] is the mass of moist soil measured directly after the extraction and Sd [g] is the mass of

256   soil dried at 105 °C for at least 24 hours. Bulk density [g cm⁻³] (BD) was calculated as following:

257    $BD = \frac{Sd}{Sv}$,   (2)

258   where Sv [cm⁻³] is the volume of the sample. Soil particle density [g cm⁻³] (SPD) was calculated as in Eq

259   (3):

260    $SPD = \frac{dm}{Sv}$,   ,   (3)

261   where dm [g] is the dry mass of soil particles.

262   Particle size distribution [%] – clay (< 0.002 mm), coarse, middle and fine silt (0.002 mm to 0.02 mm),

263   and coarse, middle and fine sand (0.02 mm to 2 mm) was estimated using a PARIO method (Durner et

264   al., 2017). Soil skeleton was estimated as the ratio of particles with a diameter above 2 mm. Ratio of

265   organic matter (OM) was estimated as in Eq. (4)

266    $OM = \frac{Sc}{Sd}$,   (4)

267   where Sc is the weight [g] of the sample dried at 500 °C for 16 hours.

268   We used pedotransfer functions to determine porosity, saturated soil moisture, hydraulic conductivity,

269   water content at field capacity, and permanent wilting point. Pore ratio (θs) was estimated from bulk and

270   particle density as in Eq. (5):

271    $\theta s = \frac{BD}{SPD}$ (5)

272   Saturated water content [g g⁻¹] (Ws) was estimated as in Eq. (6):

273    $Ws = \theta s \frac{pw}{BD}$,   (6)

274   where pw [g cm⁻³] is the density of water which is set to be 1 g cm⁻³ (Pollacco, 2008).

275   Hydraulic conductivity Ks [m s⁻¹] was estimated as in Eq. (8):

276    $Ks = 1.15741 * 0.0000001 * \exp(x)$,   (7)

277   where x for sandy soil is:

278    $x = 9.5 - 1.471 * (BD * BD) - 0.688 * OM + 0.0369 * (OM * OM) - 0.332 * CS$,   (8)

279   and x for loamy and clayey soils is:

280    $x = -43.1 + 64.8 * BD - 22.21 * (BD * BD) + 7.02 * OM - 0.1562 * (OM * OM) + 0.985 * \ln(OM) -$

281    $0.01332 * C * OM - 4.71 * BD * CS$,   (9)

282   where C is percentage of clay and CS is percentage of clay and silt (Wösten, 1997). To estimate water

283   content at field capacity [%] (FC) and permanent wilting point (PWP), we applied functions by (Tomasella

284   et al., 2000) as these were developed for South American soils:

285    $FC = 4.046 + 0.426 * Si + 0.404 * C$,   (10)

286    $PWP = 0.91 + 0.15 * Si + 0.396 * C$,   (11)

287   where Si is the percentage of silt.

288

3.3 Processing of remote sensing data

The digital elevation models (DEM) were calculated from the LiDAR data (Kügler et al., 2022; Horn, 1981) at a resolution of 0.5 m. Slope was calculated according to Horn (1981). Manning's surface roughness coefficient was estimated following (Li and Zhang, 2001). Topographic position index (TPI) and Topographic ruggedness index were calculated according to (Wilson et al., 2007). Plan and profile curvature were determined after (Zevenbergen and Thorne, 1987). Connectivity indices, Sinks, Wetness index, Flow direction, Flow path, Catchment slope and Catchment were calculated in SAGA GIS. Single license stereo WorldView-2 images with a resolution of 0.5 m were retrieved from GAF Munich GmbH. The topographic correction of WorldView-2 images was done using the LiDAR data, solar elevation angle, solar zenith angle and azimuth angle according to Goslee (2019). The digital surface models (DSMs) were calculated from the stereo images. Additionally, we extracted single bands and calculated the normalized difference vegetation index (NDVI).

3.4 The erosion model

3.4.1 Daily Morgan-Morgan-Finney model

The DMMF model is a combined soil erosion model used to estimate surface runoff and sediment flux on a field scale on a daily basis. Spatially, the DMMF model represents an area as several interconnected elements (e.g. pixels) of uniform topography, soil characteristics, land cover type, and vegetation structure. Through coupling, the model operates with flow direction algorithms: each element receives water and sediments from upslope elements and delivers the generated surface runoff and eroded soils to downslope elements. On a temporal scale, the model estimates surface runoff and sediment flux of each element on a daily basis. The model input parameters include climate, topography, soil properties and land cover information (Choi et al., 2017). Data pre-processing, modelling and analysis (see Fig. 2) was done in R statistic environment. The raster data were cropped to the size of the catchments (Fig. 1). Input parameters are listed in Table 1 and plotted in Fig. A2.

3.4.2 Estimation of spatial parameters

For spatial parameterization of the DMMF model, we upscaled land cover, soil properties and burrow distribution onto the catchments using machine learning techniques. For each parameter, we trained one random forest (RF) model per site. The upscaling was done at 0.5 m spatial resolution. We used the WorldView-2 layers, NDVI, DEM, DSM, slope and roughness as predictors while the response data were the parameters which we measured in-situ (soil properties, vegetation, burrow locations). The most important predictors were selected by forward feature selection. The quality of the random forest models was assessed by Leave-Location-Out cross validation. We trained the model stepwise, using in-situ data collected from seven of the catchments and validated the model using in-situ data from the remaining catchment (Meyer et al., 2018).

For the area-wide upscaling of burrow locations across the catchments, we used the burrow presence and absence data (section 3.1) as the response data within the RF models. The accuracy was 0.82 for PdA, 0.77 for SG, 0.75 for LC and 0.85 for NA.

328   The upscaling of soil properties was done using soil properties estimated along the track line (see
329   section 3.1) as response data within the RF models. All of the models reached a high accuracy (Table
330   A1).
331   To upscale the vegetation cover and type, we used as the response within the RF models the land cover
332   measured in-situ. The classes were soil without rocks, rocks, biocrusts, grass/herbs, shrubs and trees.
333   Predictor values for each class were extracted from at least 100 polygons per site and class. The
334   accuracy of the RF models was 0.71 for PdA, 0.81 for SG, 0.83 for LC and 0.75 for NA. The vegetation
335   height measured in plots was averaged for each class per site. All pixels classified as respective class
336   were assigned the same vegetation height information. Vegetation density was estimated per catchment
337   as the amount of vegetation individuals per m². Vegetation diversity was calculated by Shannon index
338   (Shannon, 1948). The interception area was the area not covered by vegetation (herbs, shrubs or trees).
339

3.4.3 Inclusion of bioturbation

341   In the grid cells with predicted burrow locations, we adapted the values of input parameters to include
342   bioturbation. The adaptations varied with climate zone and burrow size. The size, geometric structure
343   and excavation rates of burrowing animalswere previously estimated at a high spatial and temporal
344   resolution (Grigusova et al., 2022). Based on this results, we firstly adjusted the microtopography. We
345   modified the layer depth to represent burrow entrance and elevation to represent animal mound. Mounds
346   were always located downslope of burrow entrances in the direction of flow.
347   Secondly, we adjusted the soil properties. Soil properties texture and organic carbon were estimated
348   from soil extracted from mounds in Kraus et al. (in review). In this study we additionally estimated bulk
349   density, initial water content, soil skeleton, porosity, saturated water content, available water capacity
350   and water content at field capacity from the same dataset (see section 3.2). We calculated the median
351   value of each property for the samples extracted from mounds and for the samples extracted from soil
352   without mounds. Then, we estimated the change in percent between these two values. This was then
353   used to adjust the soil property for each pixel including a mound.
354   Thirdly, modelled mound pixels had to be cleared from ground vegetation cover. For this, we removed
355   ground vegetation cover from pixels with burrow locations and decreased ground vegetation cover,
356   height, diameter and amount of ground vegetation individuals from surrounding pixels as measured in
357   situ. Then, the amount of above-ground skeleton and debris was set as estimated from soil samples
358   (section 3.2)
359   Animal activity has been found to be highly variable throughout the year (Grigusova et al., 2022; Kraus
360   et al., 2022). The density of burrows does not stay stable throughout the year but increases or decreases
361   depending on the season and climate zone. For this, we artificially removed or added burrows into the
362   catchments at the particular seasons. Furthermore, the animals do not burrow at the same pace in the
363   course of the year. There is a 3-month period, during which they are highly active.
364   Lastly, we also included the vertical movement of sediment particles from deeper soil layers to the
365   surface in dependence on climate. The animals were found to reconstruct their burrows after each
366   rainfall event (Grigusova et al., 2022). Corresponding with these findings, we increased the entrance
367   depth and mound height by 30% after each rainfall event.
368

369 **Table 1.** Model input layers and respective changes to layer values at the predicted burrow locations.
370 Ground vegetation was removed from the respective pixels, while tree canopy was not changed. The
371 values were estimated as described in 3.5.2. Using the adjusted values, we calculated
372 Evapotranspiration using Penman-Monteith equation, surface roughness from the elevation layer, and
373 hydraulic conductivity, water content at field capacity and saturated water content using pedotransfer
374 functions.

Parameter group	Parameter	Units	Pixel value at burrow locations			
			PdA	SG	LC	NA
Topography	Elevation	m asl	+0.24	+0.23	+0.36	+0.19
	Surface roughness	-	-	-	-	-
	Depth	m	-0.23	-0.41	-0.22	-0.04
Soil	Water content	%	+120	-6	-68	-62
	Bulk density	g cm^{-3}	-	-6	-17	-
	Sand	%	-29	-12	+57	-43
	Silt	%	+54	+22	+23	ns
	Clay	%	+145	+44	+19	-73
	Organic carbon	%	+168	+72	+105	+25
	Hydraulic conductivity	m s^{-1}	-	-	-	-
	Water content at field capacity	%	-	-	-	-
	Saturated water content	%	-	-	-	-
Cover	Ground vegetation cover	%	0	0	0	0
	Soil and debris	%	100	100	100	100
	Skeleton	%	0	0	0	0
	Average plant height	m	0	0	0	0
	Average plant diameter	m	0	0	0	0
	Number of plants	n m^{-2}	0	0	0	0

375

376 **3.5 DMMF model sensitivity test and validation**

377 We conducted a sensitivity test to identify the input parameters, which significantly influence the model
378 output. For this, we estimated the mean, minimum and maximum values of each input parameter. For
379 this, we first created an artificial catchment of 100 m * 100 m. Then, each pixel received a mean value
380 of each parameter. We ran the model under these conditions. The model output described: (i) sediment
381 erosion, (ii) sediment accumulation and (iii) surface runoff. We estimated sediment redistribution by
382 subtracting the erosion from accumulation for each pixel. Then, we stepwise changed the input
383 parameter values from their minimum to their maximum values while we did not adjust any other
384 parameters. To quantify the significance of the input variations, we conducted a t-test (Fig A2). For this,
385 we compared the amount of redistributed sediment of each model run to the first model run with
386 homogeneous parameters.

387   For the validation, we ran the model for the time periods between the installation of sediment fences
388   and the collections of sediment. We compared the mass and weight of modelled and collected sediment
389   and estimated R^2 and RMSE. To test the importance of the inclusion of individual bioturbation
390   parameters into the model, we ran the model under 4 conditions: (i) No burrows; (ii) Solely entrances;
391   (iii) Solely mounds; (iv) Entire burrows (entrances and mounds).
392

393   **3.6 Impact of burrows on surface processes**
394   We estimated burrow density, as a ratio of pixels with predicted burrows to all pixels. Additionally, we
395   calculated the ratio of pixels which are part of a burrow aggregation to all pixels which include a burrow.
396   Burrow aggregation describes at least 4 neighboring pixels with predicted burrows. We calculated the
397   amount of excavated sediment as a sum of burrow density and the burrow excavation rate as estimated
398   in Grigusova et al. (2022).
399   To estimate the impact of burrows on sediment redistribution and surface runoff, we ran the DMMF
400   model for the time period from 1st April 2016 until 31th December 2021 for all catchments. We ran the
401   model (i) with no burrows and (ii) with entire burrows. We estimated (i) sediment redistribution
402   (accumulation - erosion) and (ii) surface runoff. We analyzed the redistribution and runoff on the plot (1
403   m²) and catchment (1 ha) scale.
404   Lastly, to analyze under which biotic and abiotic environmental parameters (topography, vegetation
405   cover) the bioturbation enhances sediment erosion or accumulation, we set-up a generalized additive
406   model (GAM) (Wood, 2006). For this, we first subtracted the output of the model with no burrows from
407   the output of the model with entire burrows. Positive pixel values thus meant, bioturbation enhanced
408   sediment accumulation, negative pixel values meant, bioturbation enhanced sediment erosion. We
409   tested following environmental parameters: mound density, vegetation cover, elevation, slope, aspect,
410   TRI, curvature and connectivity and wetness index. The model performance was evaluated by the
411   percentage of explained data variance. We analyzed the impact of environmental parameters within 1-
412   meter and within 10-meter distance from the burrows.
413

414   **4 Results**
415   **4.1 Model sensitivity test and accuracy**
416   Parameters which significantly influenced the model output were precipitation, slope, vegetation cover,
417   surface roughness, silt content and water content (Table A2). We quantified the model performance by
418   comparing the modelled and measured sediment redistribution. The performance varied depending on
419   the burrow inclusion (Figure 4). The performance of the model without any bioturbation was lower (R^2 =
420   0.73, RMSE = 1.50, MSE = 2.27), as when burrow entrances (R^2 = 0.81, RMSE = 1.34, MSE = 1.16) or
421   mounds (R^2 = 0.83, RMSE = 1.10, MSE = 1.22) were included. The model had the highest performance
422   when entire burrows were included (R^2 = 0.85, RMSE = 1.01, MSE = 1.01). However, as the scatterplots
423   showed, the model performance seemed to be determined strongly by one measurement (Fig. A3). For
424   this reason, we calculated the metrics without this measurement (Fig. A4). The model without any
425   burrows (R^2 = 0.17, RMSE = 1.18, MSE = 1.39) in this case performed much lower than models with
426   burrows. The model performance continuously strongly increased when burrow entrances (R^2 = 0.48,
427   RMSE = 0.61, MSE = 0.78), mounds (R^2 = 0.51, RMSE = 0.75, MSE = 0.57) were included. The model

428   with whole burrows reached the highest performance (R^2 = 0.71, RMSE = 0.63, MSE = 0.39). When we
429   compare the modelled redistribution to the sediment redistribution estimated by Time-of-Flight cameras
430   in Grigusova et al. (2022), then the differences are minor (R^2 = 0.62, RMSE = 0.12, MSE = 0.35).
431
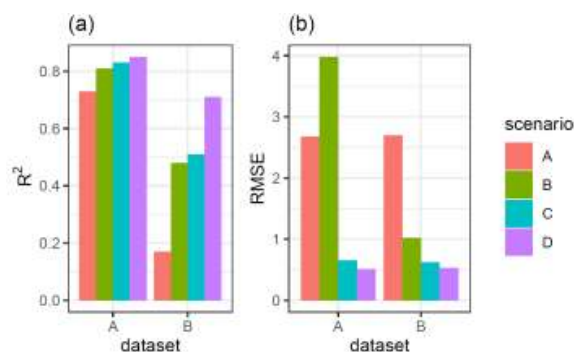
433   **Figure 4.** R^2 and RMSE of the Morgan-Morgan-Finney soil erosion model. For dataset A, we compared
434   the amount of sediment collected in all sediment fences with the modelled eroded sediment (see Fig.
435   A3). For dataset B, we removed one measurement, as the R^2 seemed to be defined by this
436   measurement (see Fig. A4). For Scenario A, we did not include any burrows into the model. For scenario
437   B, we included burrow entrances and for scenario C, we included mounds. For scenario D, we included
438   whole burrows into the model. The adjustments made to include entrances, mounds and burrows into
439   the model are described in section 3.5.2.
440

441   **4.2 Model output: Surface runoff and sediment redistribution**
442   Catchment – wide sediment redistribution (1 ha resolution) was the highest in humid NA, followed by
443   Mediterranean LC, semi-arid SG and arid PdA (Fig. 5a, 5b, 6). In NA, LC and SG, the erosion processes
444   dominated, while in PdA, more sediment accumulated than eroded. The impact of burrows on sediment
445   redistribution was significant in PdA, SG and LC. Burrows increased sediment erosion by 137.8 % in
446   PdA (3.53 kg ha^{-1} year^{-1} vs. 48.79 kg ha^{-1} year^{-1}), by 6.5 % in SG (129.16 kg ha^{-1} year^{-1} vs. 122.05 kg ha^{-1}
447   year^{-1}) and by 15.6 % in LC (4602.69 kg ha^{-1} year^{-1} vs. 3980.96 kg ha^{-1} year^{-1}).
448   Surface runoff was the highest in humid NA, followed by Mediterranean LC, arid PdA and semi-arid SG
449   (Figure 5c). The impact of burrows on surface runoff was significant in all climate zones. Burrows
450   increased surface runoff in PdA by 34 %, in SG by 40% and in LC by 4.1 %; and decreased surface
451   runoff by 5.9 % in NA. Catchment-wide maps are shown in Fig. A6-A8.
452

453

454
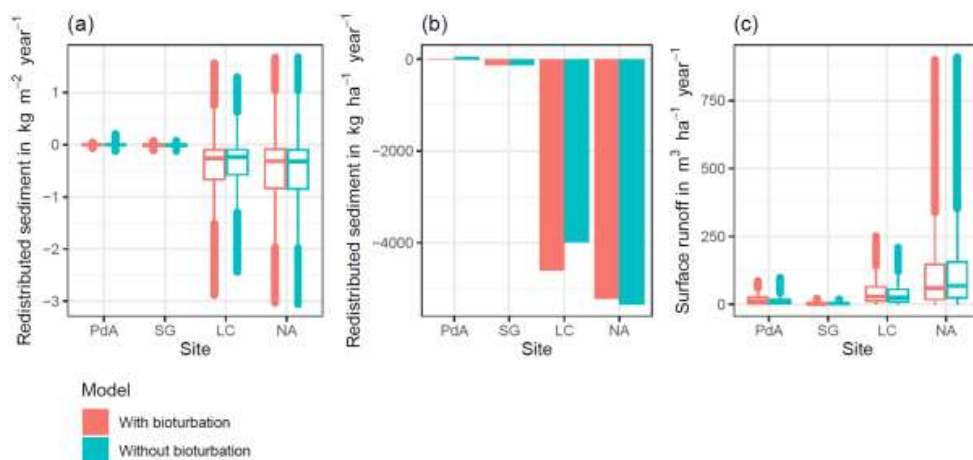
Figure 5. Summary of model outputs across the climate gradient. (a) and (b) Modelled sediment redistribution. Positive values indicate sediment accumulation; negative values indicate sediment erosion. (a) Sediment redistribution on a pixel scale in kg m^{-2} year^{-1}. (b) Sediment redistribution on the catchment scale in kg ha^{-1} year^{-1}. The impact of bioturbation on sediment redistribution was estimated by a t-test and was significant in PdA***, SG** and LC***. Bioturbation increased sediment erosion by 137.8 % in PdA, by 6.5 % in SG and by 15.6 % in LC. For catchment-wide maps see Fig. A6-A8). (c) Modelled surface runoff on the catchment scale in m^3 ha^{-1} year^{-1}. Impact of bioturbation on surface runoff was estimated by a t-test and was significant at all sites. Bioturbation increased surface runoff in PdA by 34 %, in SG by 40 % and in LC by 4.1 %; and decreased surface runoff by 5.9 % in NA. For catchment-wide maps see Fig. A6.

465
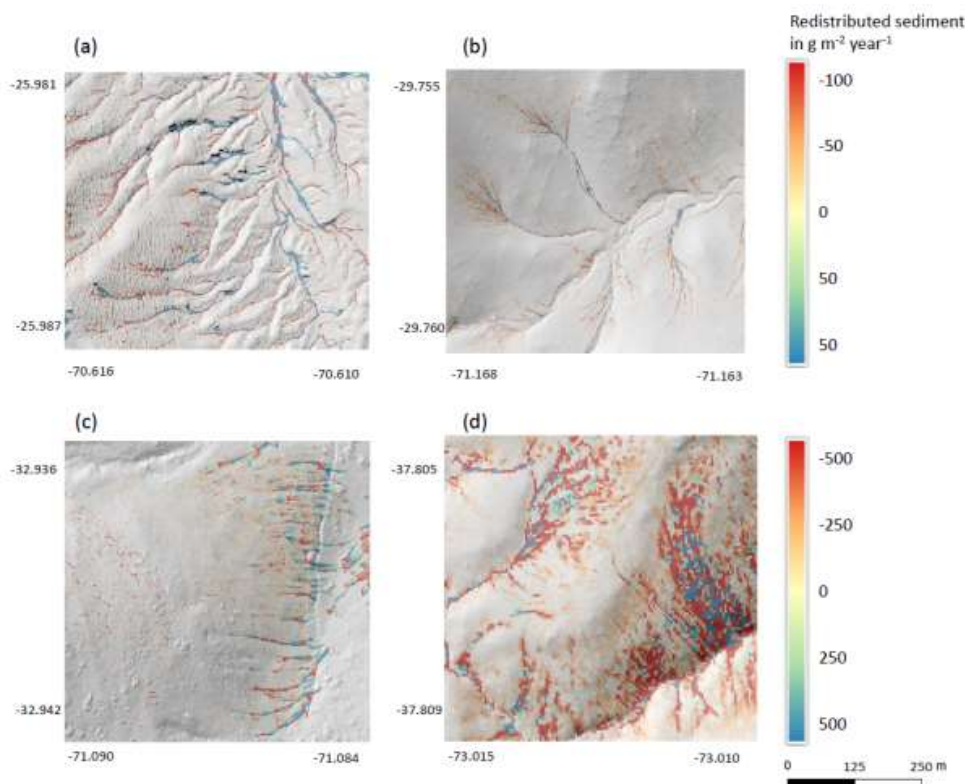
Figure 6. Catchment-wide predicted sediment redistribution. Colours indicate sediment redistribution. Positive values indicate sediment accumulation; negative values indicate sediment erosion. Grey shadows indicate the hill shading calculated from LiDAR data. (a) Pan de Azúcar, (b) Santa Gracia, (c) La Campana, (d) Nahuelbuta.

4.3 Role of continuous burrowing activity on sediment redistribution

We included the excavation of the sediment by the animal itself into the model. The density of burrows was the highest in PdA, then LC, SG and the lowest in NA (Table 2). The burrow aggregations were most predominant in LC and SG, almost non-existent in NA. The burrows were of largest size in LC, followed by PdA, SG and NA. Similarly, the highest volume of excavated sediment at the beginning of the modelling period was in LC and PdA. After each rainfall event, the animals reconstructed their burrows as described in Grigusova et al. 2022. Due to various number of rainfall events, the volume of excavated sediment during our modelling period was the highest in NA, followed by LC, SG and PdA. However, when the percentage of sediment which was excavated before and during the modelling to the amount of sediment redistributed during rainfall events was 47 % in PdA, 24 % in SG, 33.5 % in LC and 5.6 % in NA.

Table 2. Impact of animal bioturbation activity on overall sediment redistribution on various scales. The bioturbation activity was estimated using Time-of-Flight based cameras in Grigusova et al. 2022. This

486 study showed that animals reconstruct their burrows after each rainfall events. During this process, 10
487 % of the overall sediment burrow volume is relocated from within the burrow to the surface. We
488 integrated this process into our model and calculated the percentage of newly excavated sediment by
489 the animals to the amount of sediment which was redistributed during rainfalls for the period of one year.

Parameter	Units	PdA	SG	LC	NA
Burrow density	ha^{-1}	91.35	71.50	84.36	13.30
Burrow aggregations	%	24	62	73	5
Burrow size	m^3	0.015	0.012	0.047	0.008
Sediment at the surface at the start of modelling	m^3 ha^{-1}	1.35	0.88	4.11	0.10
Sediment excavated after each rainfall	m^3 ha^{-1}	0.07	0.04	0.22	0.01
Number of rainfall events	year^{-1}	3	7	16	137
Sediment excavated by the animal after the rain	m^3 ha^{-1} year^{-1}	0.21	0.28	3.52	0.69
Sediment redistributed due to rainfall	m^3 ha^{-1} year^{-1}	0.44	1.17	10.51	12.21
Excavated sediment to redistributed sediment	%	47	24	33.5	5.6

490

4.4 Role of surrounding environment
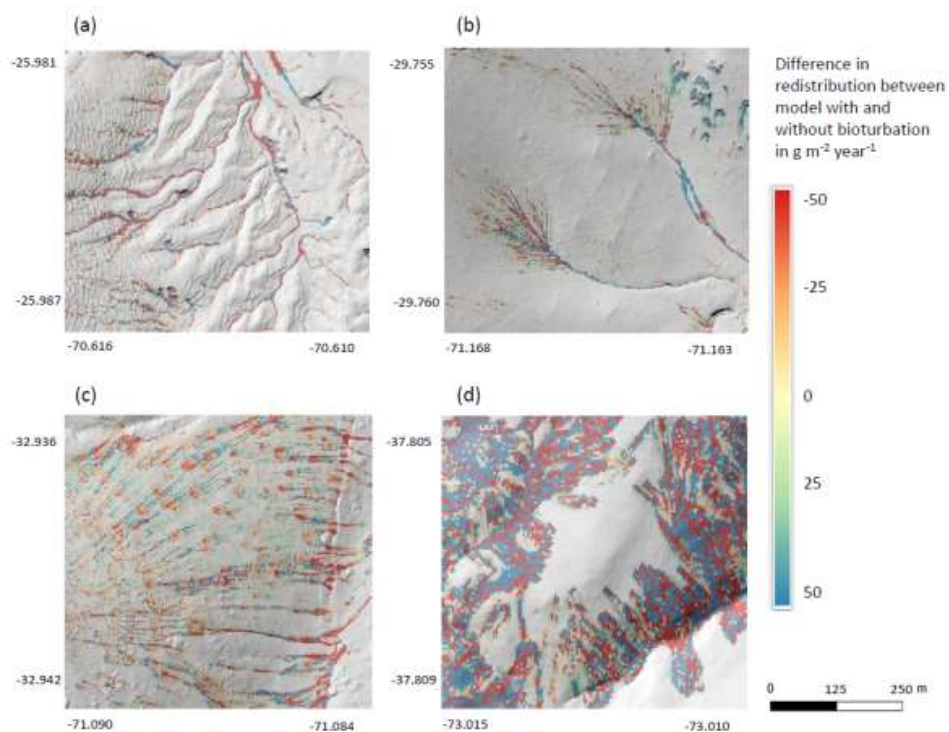
492 We subtracted the output of the model with included burrows from the output of the model without
493 burrows (Figure A8). Although, the burrows on average enhanced sediment erosion on the catchment
494 – scale, the high–resolution maps unveiled that burrows enhance sediment erosion within some pixels
495 while they rather increased sediment accumulation within others.
496 The amount of data variance explained by the GAM models (see section 3.6.) differed between models
497 (Table A3). Models estimating the impact of environmental parameters on sediment redistribution within
498 1-meter distance from the burrows, explained 3.84 % of variance in PdA, 37.1 % in SG, 46 % in LC and
499 42. % in NA. Models estimating the impact of environmental parameters on sediment redistribution
500 within 10-meter distance from the burrows, explained 1.99 % of variance in PdA, 12.8 % in SG, 52 % in
501 LC and 72.9 % in NA. The parameters selected for SG were slope, roughness, curvature, TRI and NDVI.
502 Parameters selected for LC were elevation, slope, NDVI, sinks and roughness. Parameters selected for
503 NA were elevation, slope, aspect, TRI, sinks and roughness (Table 3).
504 Bioturbation strongly increased sediment redistribution (erosion and accumulation) at high values of
505 elevation, slope, surface roughness TRI, sinks and topographic wetness index, at the middle values of
506 elevation and aspect, and at low values of profile curvature and NDVI. From these parameters,
507 bioturbation increased sediment erosion at high and middle values of elevation, at high values of slope,
508 sinks and TRI, and at low values of profile curvature. Bioturbation increased sediment accumulation at
509 high values of surface roughness and topographic wetness index and at low values of NDVI (Fig. A9 –
510 A14).
511 Bioturbation somewhat enhanced sediment erosion at medium values of surface roughness, NDVI and
512 sinks, and at low values of topographic wetness index. Bioturbation somewhat increased sediment
513 accumulation at low values of slope and TRI, at low and medium values of elevation and at high values
514 of profile curvature.
515

Figure 7. Catchment-wide impact of bioturbation on sediment redistribution. Colour indicates the impact. Positive values indicate bioturbation enhanced sediment accumulation, negative values indicate bioturbation enhanced sediment erosion. Grey shadows indicate the hill shading calculated from LiDAR data. (a) Pan de Azúcar, (b) Santa Gracia, (c) La Campana, (d) Nahuelbuta.
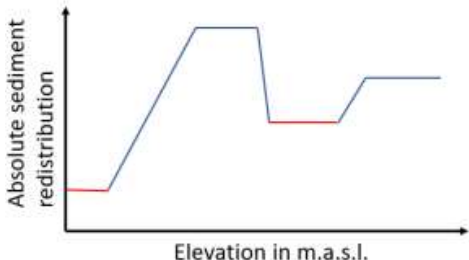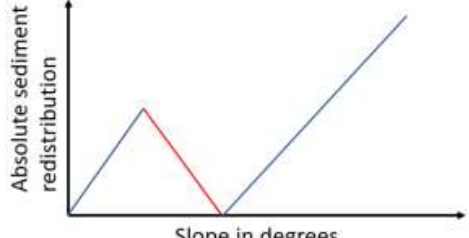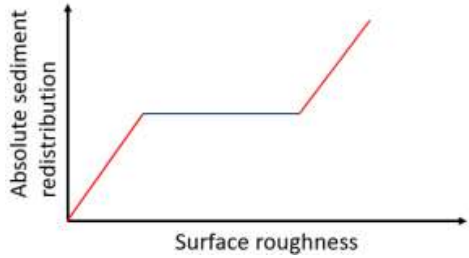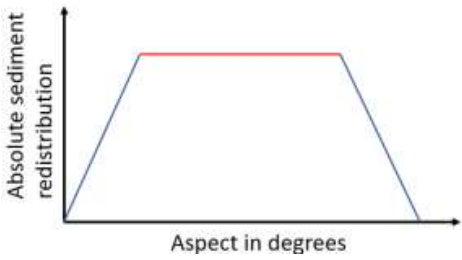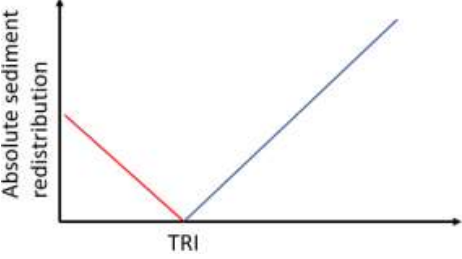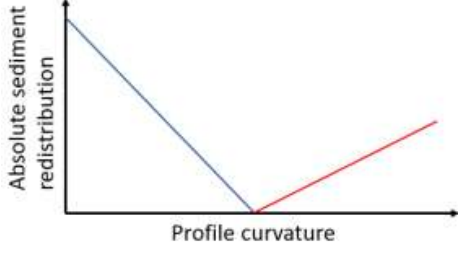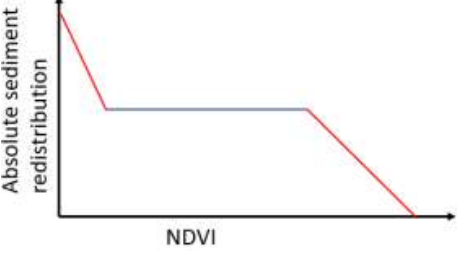
537 **Table 3.** Parameters influencing impact of bioturbation on sediment redistribution. The catchment-wide
538 analysis showed that bioturbation has varying impact on sediment redistribution (see Fig. 5,7). The x-
539 axis shows the parameter values. The y-axis shows the amount of sediment which was redistributed
540 due to bioturbation. Red colour indicates that at these parameter values, bioturbation caused sediment
541 accumulation. Blue colour indicates that at these parameter values, bioturbation enhanced sediment
542 erosion. One GAM model was run per site. The lines are not smooth as this is a conceptual figure only.
543 For regression fits as estimated by the GAMs see Fig. A9-A14. For the amount of explained variance of
544 each GAM model see Tab. A2.

Parameter	Impact
Elevation	
Slope	
Surface roughness	

Aspect	
TRI	
Profile curvature	
NDVI	

545
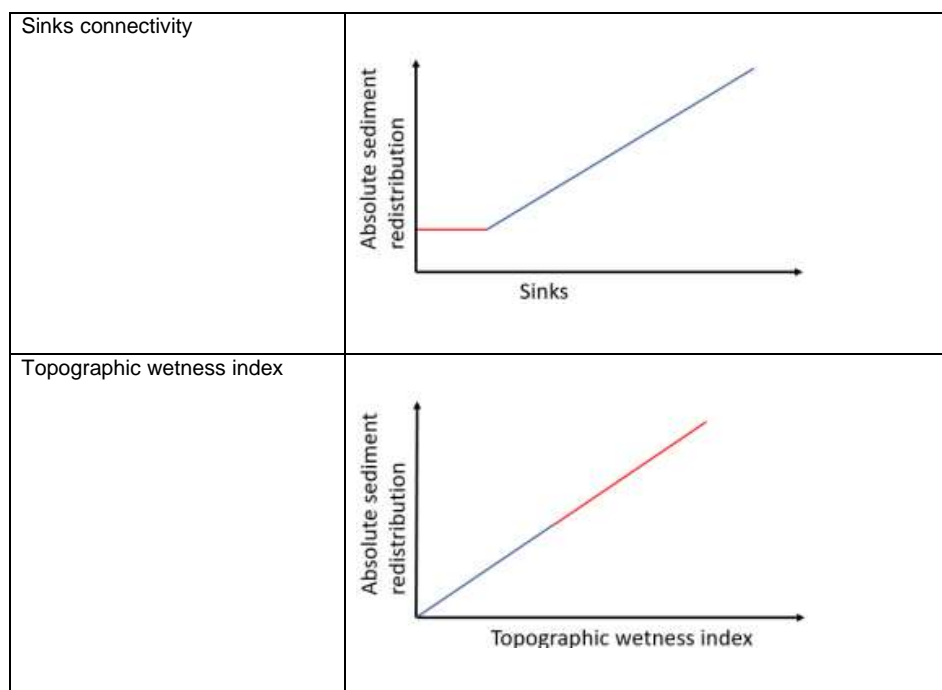
5. Discussion

5.1 The inclusion of bioturbation increases model performance

548 Overall, our DMMF model including bioturbation performed much better than the model without

549 bioturbation. The DMMF model without bioturbation performed worse (RMSE of 1.18 kg ha^{-1} year^{-1} and

550 R^2 of 0.17) than the model with bioturbation (RMSE was 0.63 kg ha^{-1} year^{-1} and R^2 was 0.71).

551 We hence argue that the higher accuracy of our model can be explained with the inclusion of

552 bioturbation. This is confirmed by the fact that our model run without bioturbation performed similarly to

553 previously run models without bioturbation: In earlier studies, the accuracy of the MMF model reached

554 an RMSE in between 4.9 and 8.2 kg ha^{-1} year^{-1}, with an estimated R^2 of in between 0.21 and 0.57 (Jong

555 et al., 1999; Vigiak et al., 2005; López-Vicente et al., 2008; Vieira et al., 2014; Choi et al., 2017).

556 However, we acknowledge that previous studies were all conducted in more temperate climate zones.

557 To be able to compare our results with previous studies, we calculated the model performance

558 considering solely the Mediterranean and humid climate zone. Here, our model performed better than

559 when we considered all climate zones (R^2 = 0.72, RMSE = 0.45 kg ha^{-1} year^{-1}), confirming the conclusion

560 that bioturbation increased model performance. Additionally, we compared the model output with the

561 values on sediment redistribution estimated in previous studies. Again, these were solely conducted in

562 more humid climate regions. In the humid zone, our model predicted an erosion up to 3.5 kg m^{-2} year^{-1}.

563 This estimation is in line with erosion rates due to bioturbation established by in-situ measurements in

564 other studies (between 1.5 kg m^{-2} year^{-1} and 3.7 kg m^{-2} year^{-1}) (Black and Montgomery, 1991; Yoo and

565 Mudd, 2008; Yoo et al., 2005; Rutin, 1996). This also confirms the reliability of our approach.

566

5.2 The relevance of bioturbation for sediment redistribution depends on the landscape context

On the catchment scale (1 ha), our study finds that bioturbation increases erosion in all climatic zones except within the humid zone (Figure 5b). In contrast, bioturbation increases both, erosion and accumulation, on the plot scale (1 m^2) (Figure 5a). On this scale, in the arid and semi-arid zone, sediment erosion and accumulation were predicted to be about equal ((erosion and accumulation both up to 0.1 kg m^{-2} year^{-1} in the arid zone, and erosion and accumulation both up to 0.2 kg m^{-2} year^{-1} in the semi-arid zone (see Figure 5a)). Bioturbation marginally increased erosion and decreased accumulation in the semi-arid zone, but reduced by twofold the accumulation in the arid zone. In contrast, in the Mediterranean and humid zone, erosion was predicted to be almost double when compared to accumulation (predicted erosion up to 2.5 kg m^{-2} year^{-1}, and accumulation up to 1.4 kg m^{-2} year^{-1}). Inclusion of bioturbation increased erosion up to 3 kg m^{-2} year^{-1}, and accumulation up to 1.6 kg m^{-2} year^{-1} in the Mediterranean zone, while it had no significant effect in humid zone. We argue that sediment redistribution due to bioturbation is heavily influenced by meso-topographic structures which determine the creation of surface runoff. Due to this, the erosion and accumulation on the plots scale is heavier impacted by bioturbation with increasing surface runoff.

According to our analysis, bioturbation increases erosion or accumulation of sediment mostly based on an interplay between topographic structures elevation, slope and TRI (Table 3). Over all research sites, this study found that bioturbation leads to an increase in surface erosion in areas where erosional processes dominate (upper, and/or steeper slopes), and tends to increase sediment accumulation in areas where sediment is naturally deposited, e.g. lower slopes or shallow depressions (Figure 8). This finding is based on the fact that erosion in general is positively affected by slope, and negatively by surface roughness and vegetation (Rodríguez-Caballero et al., 2012; Wang et al., 2013; Kirols et al., 2015). Additionally, the redistribution of sediment is largely affected by topographic meso-/macroforms, such as rills or cliffs. These can be quantified by topographic ruggedness index (TRI) which describes the amount of elevation drop between adjusting cells of DEM (Wilson et al., 2007). At high values of this index, we would therefore expect high erosion rate, due to concentrated runoff within the connected rills or undisturbed flow of runoff from the cliffs downslope.

Our data show that one burrow provides up to 0.43 m^3 of additional loose sediment at the surface (Table 2), while the surface roughness increases up to 200 % (Grigusova et al., 2022). When including burrows into the model, at the slope values from 0 to 5 degrees, the presence of burrows had no impact on sediment redistribution. From 5 degrees onwards it increased sediment erosion proportionally to the slope of the hillside (an increased erosion from 0.4 g ha^{-1} year^{-1} in the semi-arid zone until up to 150 kg ha^{-1} year^{-1} in the Mediterranean zone, Fig. A9 and A12). Similarly, at locations with sudden elevation drops 0 m until 0.2 m (lower TRI values), the presence of burrows had no impact. However, at locations with elevation drops of 0.2 until 0.5 m (higher TRI values), bioturbation increases sediment erosion by 1.5 kg ha^{-1} year^{-1} (Fig. A9, A12-A14). Lastly, bioturbation proportionally increased accumulation when the surface roughness values were above 0.5 (an increased accumulation from 0.2 g ha^{-1} year^{-1} in semi-arid zone until 5000 kg ha^{-1} year^{-1} in the Mediterranean zone, Fig. A9 and A12).

We conclude that in locations with slope values over 5 degrees, or at locations with sudden drops in elevation (high TRI) and connected rills, more sediment is eroding than accumulating. Here, additional surface sediments generated by bioturbators provides more source material for erosion and thus

608   bioturbation increases sediment erosion at these locations (Table 3). In contrast, at locations with a
609   slope below 5 degrees, where processes are dominantly controlled by surface roughness, sediment
610   accumulation caused by bioturbation increases proportionally when the surface roughness has a value
611   above 0.5. This is likely because burrows through their above-ground structures heavily increase surface
612   roughness (Grigusova et al., 2022), and hence the presence of bioturbating animals leads to an increase
613   in sediment accumulation.

614   Additionally, we hypothesize that it is not only the additional availability of sediment on the surface and
615   the topography of the vicinity which controls the contribution of bioturbation to sediment surface flux, but
616   also the spatial distribution of animal burrows. We interpret that in locations with high burrow
617   aggregation, surface flow might be redirected and centralized around the aggregates and thus increase
618   the sediment erosion in the areas surrounding burrow aggregates (Figure A15). This mechanism could
619   explain, why bioturbation promotes sediment erosion especially in the Mediterranean zone. The relative
620   role of burrow aggregation should be studied in detail and included in future studies.
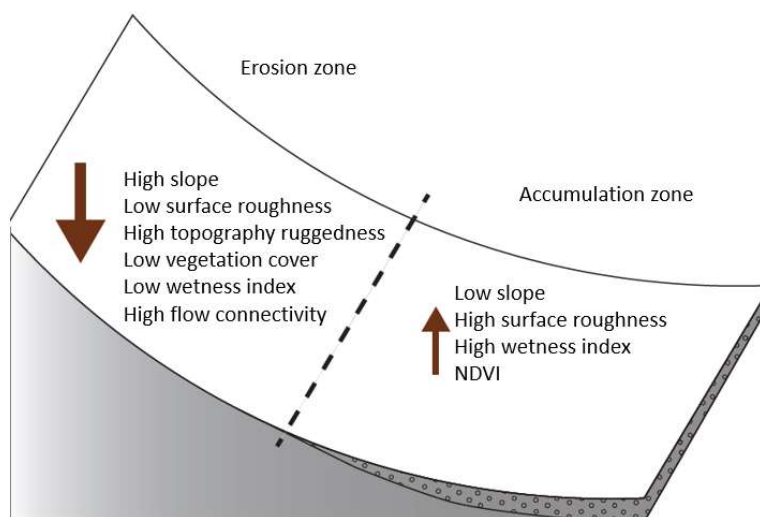
621

622   **Figure 8.** Bioturbation amplifies erosion within the erosion zone and accumulation within the
623   accumulation zone. The zones were defined based on the values of surrounding environmental
624   parameters. The arrow direction indicates decrease or increase of sediment amount within a pixel and
625   thus erosion or accumulation. The arrow thickness indicates the amount of redistributed sediment.
626   Please note that the location of the erosion zone on the upper hillside and of the accumulation zone on
627   the lower hillside is purely conceptual. Should the respective values of environmental parameters listed
628   for the erosion zone be found on the lower hillside, it would still be erosion zone. Vice versa for the
629   accumulation zone. The importance of the parameters is ranked and described in section 5.3.

630

631

632   **6. Conclusion**

633   In summary, our results show that the presence of animal burrows leads to an increase in erosion and
634   net sediment loss. According to our results, bioturbation enhances sediment erosion in areas where

635   more erosion is expected and enhances sediment accumulation in areas which are more prone to
636   accumulate sediment.
637   On geological time scales, as burrowing animals increase both, erosion in steeper zones, and
638   accumulation in areas with gentler slopes and higher roughness, hillslope relief should become faster
639   equalised and overall more flat. This tendency is the most pronounced in the Mediterranean zone with
640   high burrow density and excavation rates, as well as high precipitation rates. Our study furthermore
641   shows that the impact of bioturbation heavily depends on the surrounding environmental parameters.
642
643   **Funding:** This study was funded by the German Research Foundation, DFG [grant numbers
644   BE1780/52-1, LA3521/1-1, FA 925/12-1, BR 1293-18-1], and is part of the DFG Priority Programme
645   SPP 1803: EarthShape: Earth Surface Shaping by Biota, sub-project "Effects of bioturbation on rates
646   of vertical and horizontal sediment and nutrient fluxes".
647   **Institutional Review Board Statement:** Not applicable.
648   **Informed Consent Statement:** Not applicable.
649   **Acknowledgments:** We thank CONAF for the kind support provided during our field campaign.
650   **Competing interests:** There is no conflict of interest.
651   **Author contribution:** PG set up the model, analysed the data and wrote the manuscript draft; PG and
652   AL performed the measurements AL, JB, NF, RB, DK, PP, LP, CdR reviewed and edited the manuscript.
653   **Code/Data availability:** Code and all raw data can be provided by the corresponding author upon
654   request.
655   **Special Issue statement:** I would like to stress that the submission should be part of the Copernicus
656   special Issue (Earth surface shaping by biota (ESurf/BG/ESD/ESSD/SOIL inter-journal SI) initiated by
657   the EarthShape consortium.
658
659

660
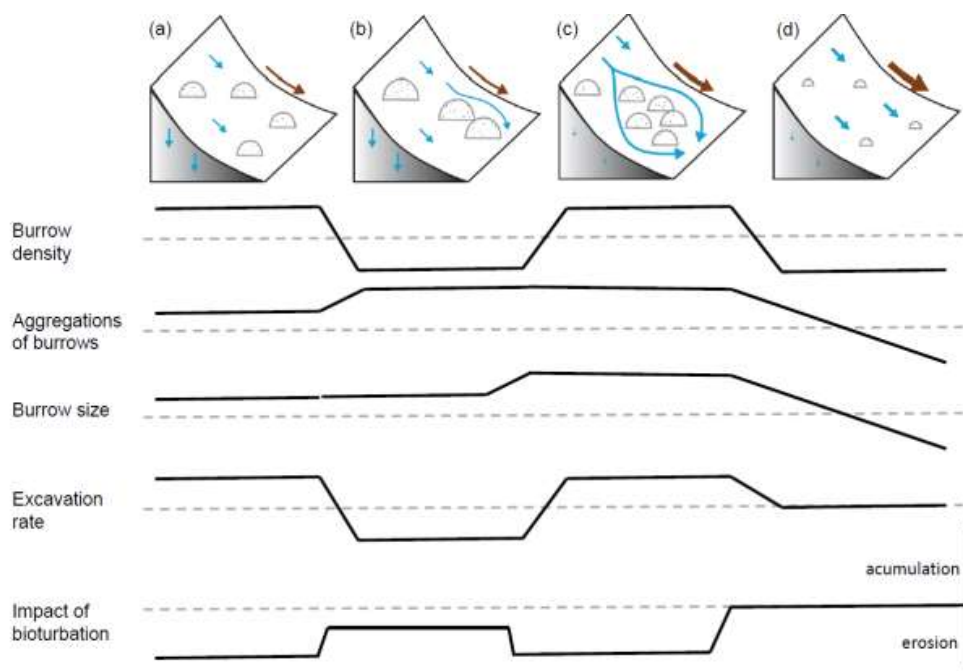
Figure 9. Context dependency of sediment redistribution. (a) Pan de Azúcar, (b) Santa Gracia, (c) La
Campana, (d) Nahuelbuta. Brown arrows indicate the direction and magnitude of overall sediment
redistribution within each climate zone. Blue arrows indicate the direction of flow (runoff vs. infiltration).
Half-moons indicate the distribution and size of burrows. The dashed line indicates the median value of
each parameter for the first four parameters.

666

Supplementary material

Table A1: R^2 and RMSE of random forest models trained for the prediction of soil properties needed for
model parametrization. RMSE is root mean square error.
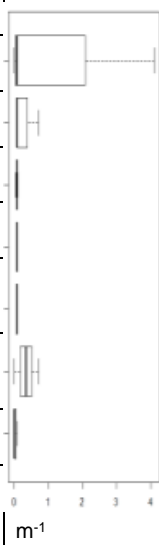
Variable	R^2	RMSE
Soil water content	0.80	0.05
Bulk density	0.60	0.22
Porosity	0.63	0.09
Silt	0.64	0.04
Middle silt	0.64	0.04
Sand	0.68	0.09
Middle sand	0.64	0.05
Organic components	0.77	0.05
Organic carbon	0.70	0.03

670

671

672 **Table A2.** Model sensitivity analysis. For the analysis, the minimum, maximum and mean value of each

673 parameter was calculated. The model was run for a catchment of 1km² with homogenous mean

674 parameters. Then, the minimum and maximum values of each parameter were tested. Each parameter

675 was stepwise changed to its minimum or maximum value while the remaining parameters stayed

676 homogenous. The significance of the parameter was estimated by a t-test conducted between the

677 erosion estimated by the model with homogenous mean parameters and the erosion estimated by the

678 model with varying minimum and maximum parameter values. Only significant parameters are shown.

Abbreviation	Parameter	mean value	min value	max value	mean erosion	min erosion	max erosion	
R	precipitation	19.9	0.2	65.6	0.07	0	4.1	
P_c	clay content	10.61	3.87	34.64	0.07	0.07	0.07	
P_z	silt content	38.49	13.32	59.59	0.07	0.04	0.11	
P_s	sand content	47.04	24.13	79.17	0.07	0.07	0.07	
theta_init	water content	3.87	2.38	12.68	0.07	0.09	0.06	
n_s	roughness	0.97	0	236.75	0.07	0.34	0.01	
GC	vegetation	79.54	50.38	92.48	0.07	0.01	0.004	
DEM	Slope of DEM	18.21	0	89.78	0.07	0	inf.	

679

680

681 **Table A3.** Summary of GAM models. We analyzed the impact of parameters within a 1-meter and 10-

682 meter distance from burrows. The Stars indicate p-values of the selected parameters. p*** < 0.001, p**

683 < 0.01, p* < 0.05, p. < 0.1. One GAM model was run per parameter. Only results for models with an

684 explained variance above 5 % are shown.

Parameters	Within 1 meter from burrows				Within 10 meters from burrows			
	PdA	SG	LC	NA	PdA	SG	LC	NA
Explained Variance	3.8 %	37 %	46 %	42 %	2.0 %	13 %	52 %	73 %
Burrow density	.				.			
Elevation			***	***	*		*	***
Slope		***					*	**
Aspect	.	**		*	*			.
Roughness		***					**	*
TPI								

TRI		**		**			
Plan curvature		.					.
Profile curv.		**	.				
NDVI			**			**	.
Sinks			*	***	*		*
Wetness				**			
Flow direction							
Flow path							
Catchment		*			*		
Catchment slope		***		.			

685

686

687
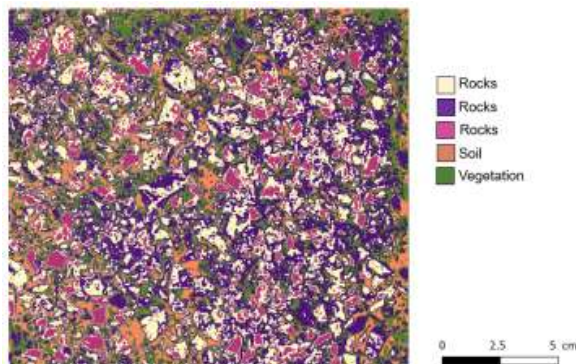
Figure A1. Example of the unsupervised k-means classification of the surface photo from La Campana. Original photo was taken by Paulina Grigusova. The collection of in-situ data is explained in section 3.1., the estimation of soil properties in section 3.2. The image was classified into 5 classes using unsupervised k-means classification; the land cover was then assigned manually. In some cases, like in this case for rocks, multiple k-means classes stand for the same land cover. These were then unified to the class "rocks".

694

695
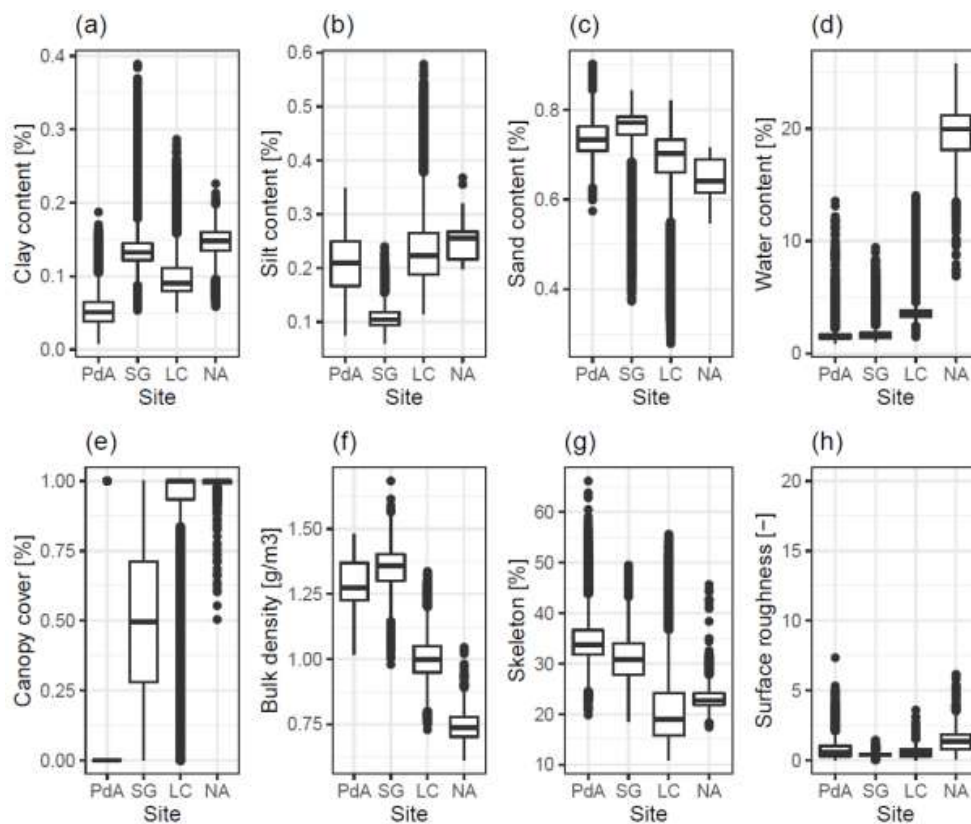
Figure A2. Input parameter values per site. The barplots show all pixel values within the researched

697 catchments for each site. The seemingly black lines outside of whiskers are as well outliers.

698
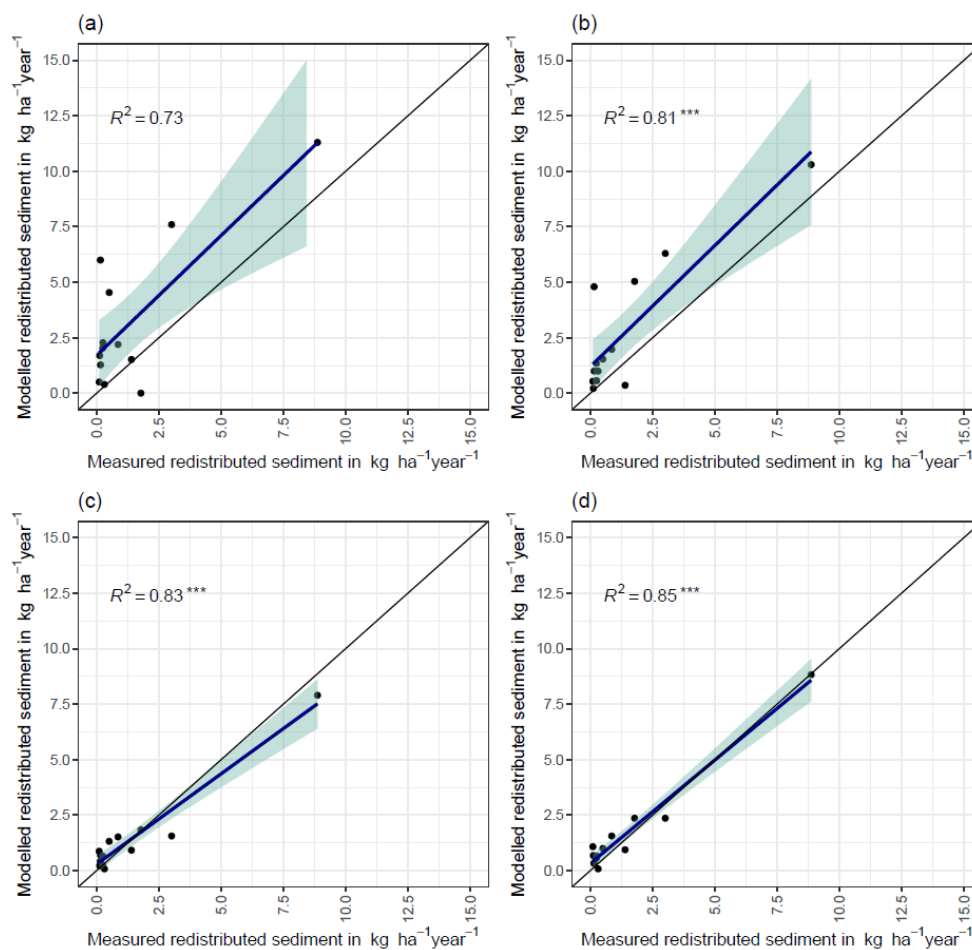
Figure A3. Measured and modelled redistributed sediment for different scenarios. (a) Model without bioturbation. (b) Model with entrances. (c) Model with mounds. (d) model with burrows.
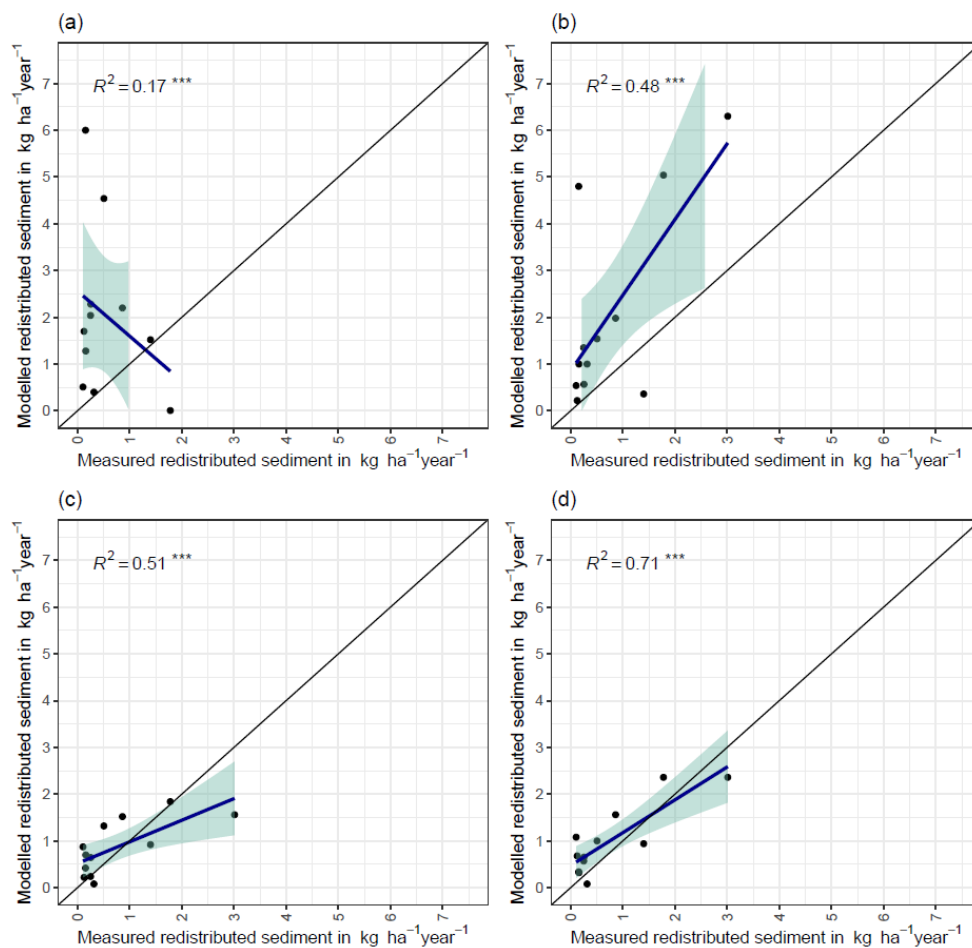
Figure A4. Measured and modelled redistributed sediment without an outlier. (a) Model without bioturbation. (b) Model with entrances. (c) Model with mounds. (d) model with burrows.
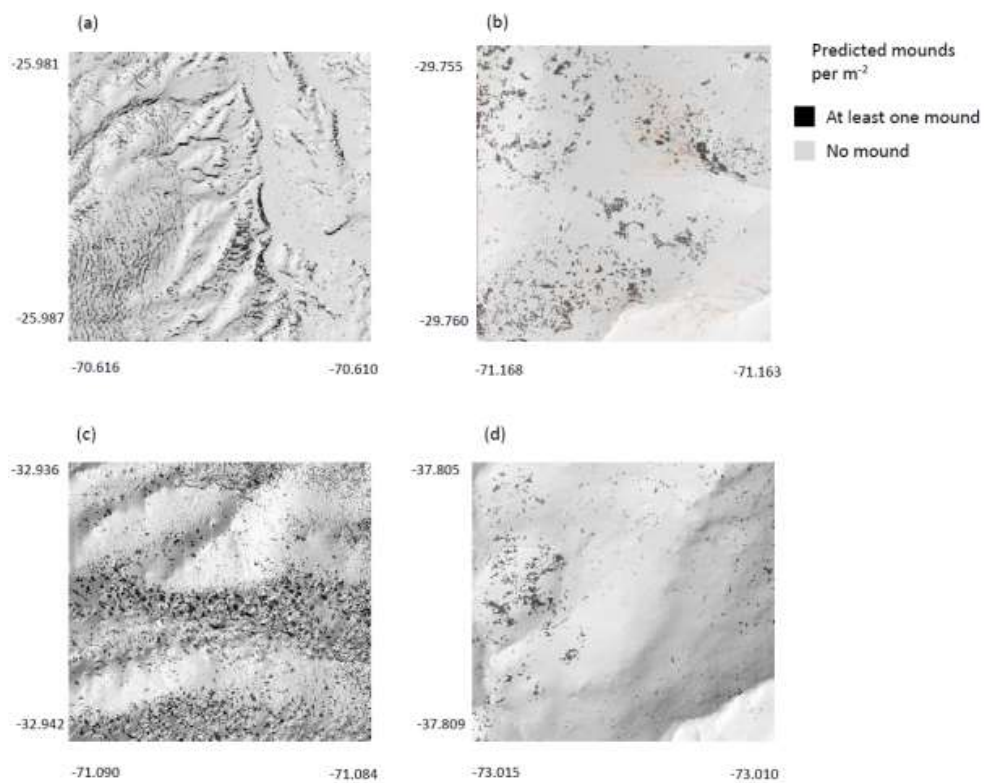
Figure A5. Predicted mounds in all climate zones. (a) Pan de Azúcar, (b) Santa Gracia, (c) La Campana, (d) Nahuelbuta. Grey shadows indicate the hill shading calculated from LiDAR data.
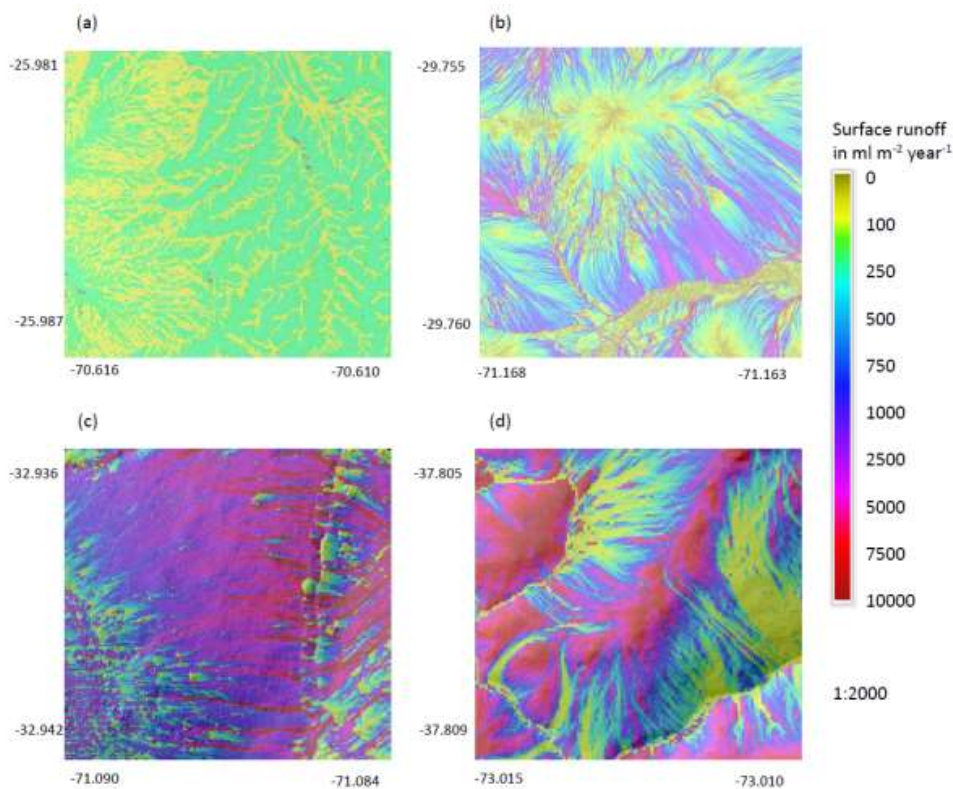
Figure A6. Catchment-wide predicted surface runoff. Colors indicate surface runoff. (a) Pan de Azúcar, (b) Santa Gracia, (c) La Campana, (d) Nahuelbuta. Grey shadows indicate the hill shading calculated from LiDAR data.
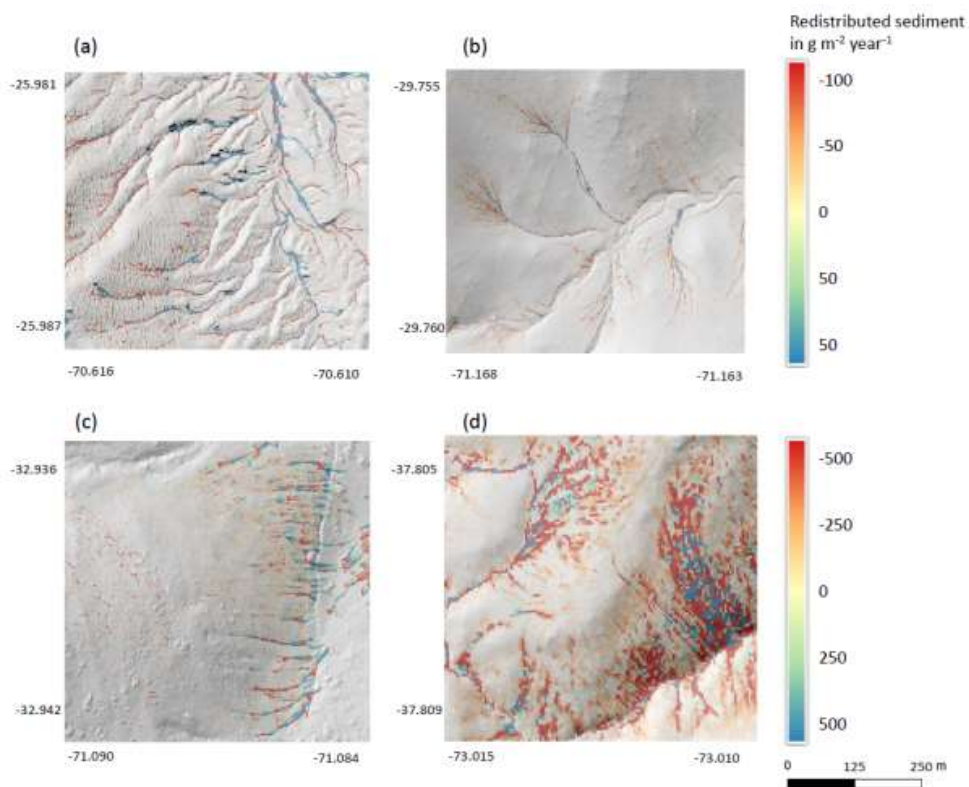
Figure A7. Catchment-wide predicted sediment redistribution. Colours indicate sediment redistribution. Positive values indicate sediment accumulation; negative values indicate sediment erosion. Grey shadows indicate the hill shading calculated from LiDAR data. a) Pan de Azúcar, (b) Santa Gracia, (c) La Campana, (d) Nahuelbuta.

Figure A8. Catchment-wide impact of bioturbation on sediment redistribution. Colour indicates the impact. Positive values indicate bioturbation enhanced sediment accumulation, negative values indicate bioturbation enhanced sediment erosion. Grey shadows indicate the hill shading calculated from LiDAR data. (a) Pan de Azúcar, (b) Santa Gracia, (c) La Campana, (d) Nahuelbuta.
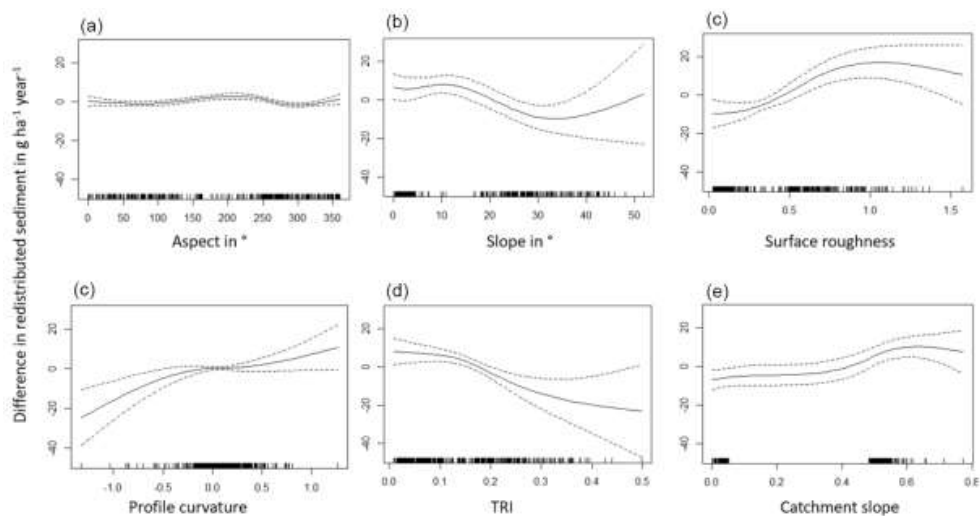
732 **Figure A9.** Environmental parameters influencing impact of bioturbation on sediment redistribution in
733 Santa Gracia within 1-meter distance from burrows. Positive values indicate bioturbation enhances
734 sediment accumulation at the respective parameter values, negative values indicate bioturbation
735 enhances sediment erosion at the respective parameter values.
736
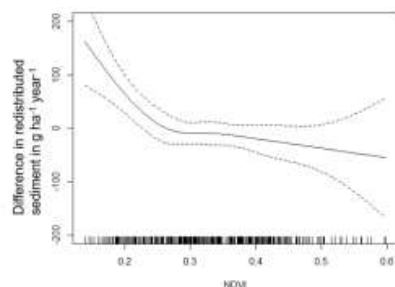
737

738 **Figure A10.** Environmental parameters influencing impact of bioturbation on sediment redistribution in
739 Santa Gracia within 10-meter distance from burrows. Positive values indicate bioturbation enhances
740 sediment accumulation at the respective parameter values, negative values indicate bioturbation
741 enhances sediment erosion at the respective parameter values.
742

743
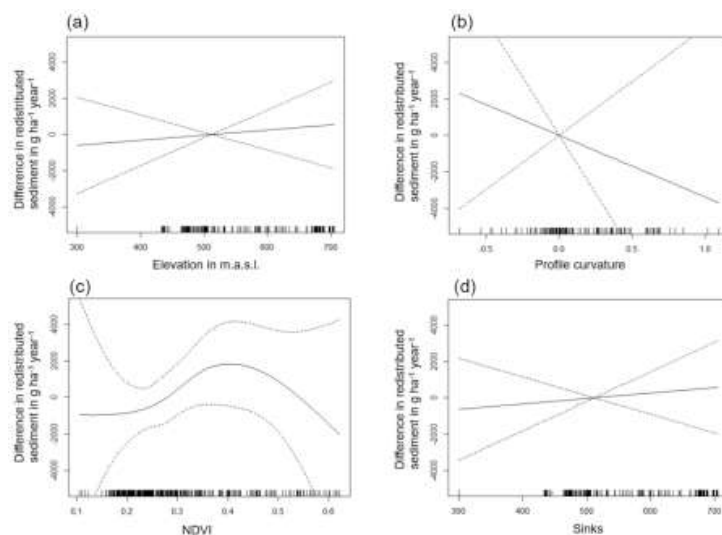
744

745 **Figure A11.** Environmental parameters influencing impact of bioturbation on sediment redistribution in
746 La Campana within 1-meter distance from burrows. Positive values indicate bioturbation enhances
747 sediment accumulation at the respective parameter values, negative values indicate bioturbation
748 enhances sediment erosion at the respective parameter values.
749
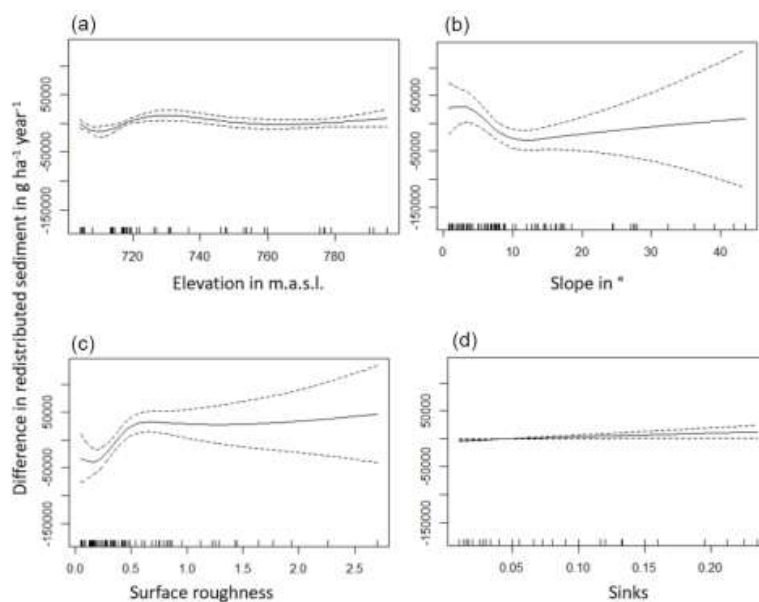
Figure A12. Environmental parameters influencing impact of bioturbation on sediment redistribution in La Campana within 10-meter distance from burrows. Positive values indicate bioturbation enhances sediment accumulation at the respective parameter values, negative values indicate bioturbation enhances sediment erosion at the respective parameter values.
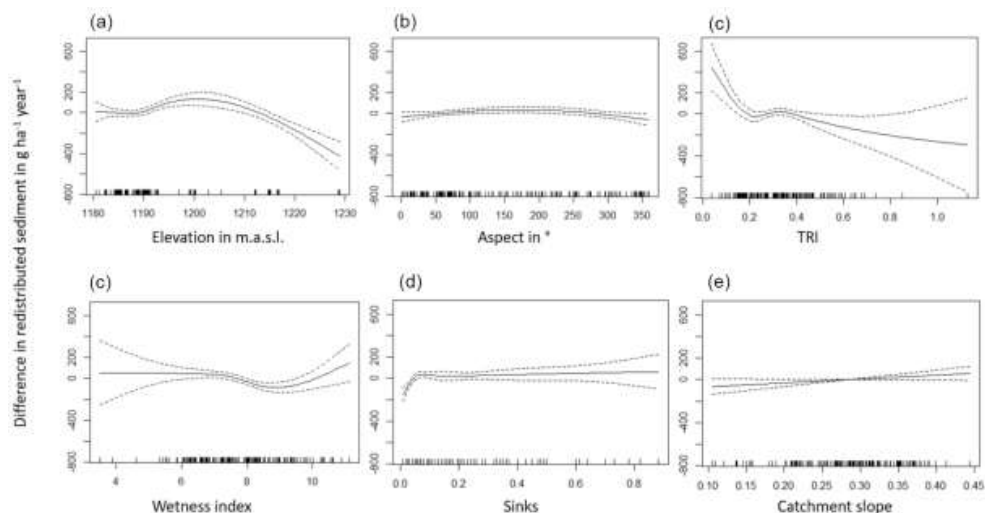
Figure A13. Environmental parameters influencing impact of bioturbation on sediment redistribution in Nahuelbuta 1-meter distance from burrows. Positive values indicate bioturbation enhances sediment accumulation at the respective parameter values, negative values indicate bioturbation enhances sediment erosion at the respective parameter values.
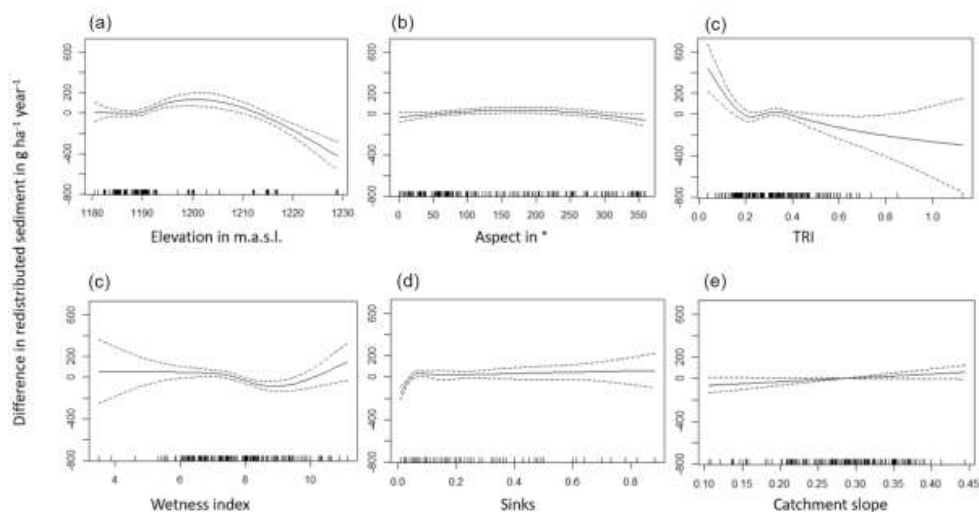
Figure A14. Environmental parameters influencing impact of bioturbation on sediment redistribution in Nahuelbuta 10-meter distance from burrows. Positive values indicate bioturbation enhances sediment accumulation at the respective parameter values, negative values indicate bioturbation enhances sediment erosion at the respective parameter values.
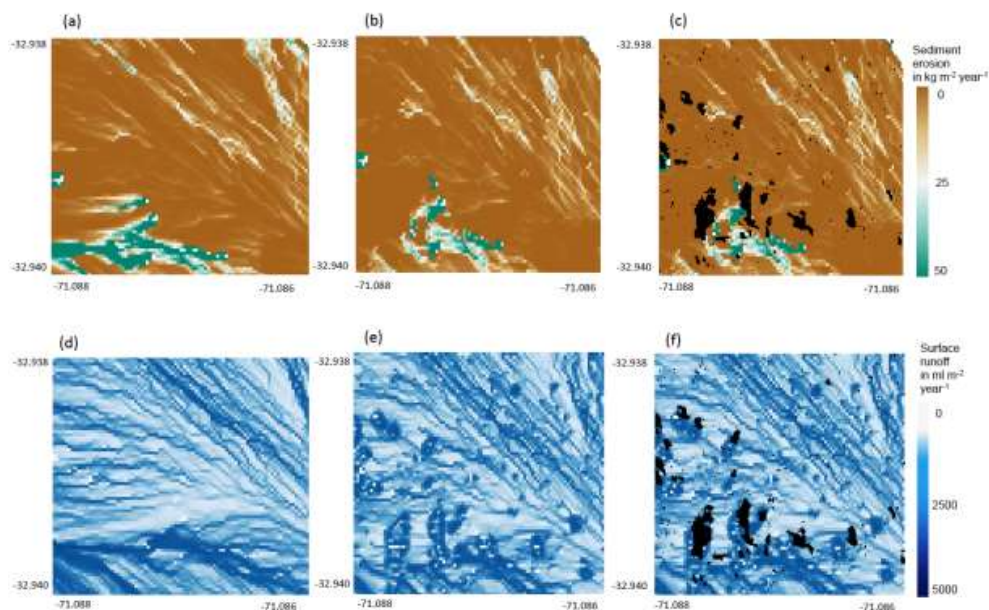
Figure A15. Burrow aggregation concentrates the runoff and increases erosion. Example for the north-facing hillside in Mediterranean La Campana for the time period of one year. (a) Sediment erosion as estimated by model without bioturbation. (b) Sediment erosion as estimated by model with bioturbation. (c) Sediment erosion as estimated by model with bioturbation with predicted burrow locations. (d) Surface runoff as estimated by model without bioturbation. (e) Surface runoff as estimated by model

774   with bioturbation. (f) Surface runoff as estimated by model including bioturbation and predicted burrow

775   locations. Black colour indicates, at least one burrow was located within this pixel. Four neighbouring

776   pixels which contain a burrow form a burrow aggregation.

777

778   References

779   Anderson, R. S., Rajaram, H., and Anderson, S. P.: Climate driven coevolution of weathering profiles
780   and hillslope topography generates dramatic differences in critical zone architecture, Hydrol.
781   Process., 33, 4–19, https://doi.org/10.1002/hyp.13307, 2019.

782   Beasley, D. B., Huggins, L. F., and Monke, E. J.: ANSWERS: A Model for Watershed Planning,
783   Transactions of the ASAE, 23, 938–944, https://doi.org/10.13031/2013.34692, 1980.

784   Bernhard, N., Moskwa, L.-M., Schmidt, K., Oeser, R. A., Aburto, F., Bader, M. Y., Baumann, K.,
785   Blanckenburg, F. von, Boy, J., van den Brink, L., Brucker, E., Büdel, B., Canessa, R., Dippold, M.
786   A., Ehlers, T. A., Fuentes, J. P., Godoy, R., Jung, P., Karsten, U., Köster, M., Kuzyakov, Y.,
787   Leinweber, P., Neidhardt, H., Matus, F., Mueller, C. W., Oelmann, Y., Oses, R., Osses, P., Paulino,
788   L., Samolov, E., Schaller, M., Schmid, M., Spielvogel, S., Spohn, M., Stock, S., Stroncik, N.,
789   Tielbörger, K., Übernickel, K., Scholten, T., Seguel, O., Wagner, D., and Kühn, P.: Pedogenic and
790   microbial interrelations to regional climate and local topography: New insights from a climate
791   gradient (arid to humid) along the Coastal Cordillera of Chile, CATENA, 170, 335–355,
792   https://doi.org/10.1016/j.catena.2018.06.018, 2018.

793   BEVEN, K. J. and KIRKBY, M. J.: A physically based, variable contributing area model of basin
794   hydrology / Un modèle à base physique de zone d'appel variable de l'hydrologie du bassin versant,
795   Hydrological Sciences Bulletin, 24, 43–69, https://doi.org/10.1080/02626667909491834, 1979.

796   Black, T. A. and Montgomery, D. R.: Sediment transport by burrowing mammals, Marin County,
797   California, Earth Surf. Process. Landforms, 16, 163–172, https://doi.org/10.1002/esp.3290160207,
798   1991.

799   Boudreau, B. P.: Mathematics of tracer mixing in sediments; I, Spatially-dependent, diffusive mixing,
800   American Journal of Science, 286, 161–198, https://doi.org/10.2475/ajs.286.3.161, 1986.

801   Boudreau, B. P.: The diffusion and telegraph equations in diagenetic modelling, Geochimica et
802   Cosmochimica Acta, 53, 1857–1866, https://doi.org/10.1016/0016-7037(89)90306-2, 1989.

803   Braun, J., Mercier, J., Guillocheau, F., and Robin, C.: A simple model for regolith formation by chemical
804   weathering, J. Geophys. Res. Earth Surf., 121, 2140–2171, https://doi.org/10.1002/2016JF003914,
805   2016.

806   Brosens, L., Campforts, B., Robinet, J., Vanacker, V., Opfergelt, S., Ameijeiras-Mariño, Y., Minella, J.
807   P. G., and Govers, G.: Slope Gradient Controls Soil Thickness and Chemical Weathering in
808   Subtropical Brazil: Understanding Rates and Timescales of Regional Soilscape Evolution Through
809   a Combination of Field Data and Modeling, J. Geophys. Res. Earth Surf., 125, 1,
810   https://doi.org/10.1029/2019JF005321, 2020.

811   Carretier, S., Goddéris, Y., Delannoy, T., and Rouby, D.: Mean bedrock-to-saprolite conversion and
812   erosion rates during mountain growth and decline, Geomorphology, 209, 39–52,
813   https://doi.org/10.1016/j.geomorph.2013.11.025, 2014.

814   Cerqueira, R.: The Distribution of Didelphis in South America (Polyprotodontia, Didelphidae), Journal of
815   Biogeography, 12, 135, https://doi.org/10.2307/2844837, 1985.

816   Chen, M., Ma, L., Shao, M.'a., Wei, X., Jia, Y., Sun, S., Zhang, Q., Li, T., Yang, X., and Gan, M.: Chinese
817   zokor (Myospalax fontanierii) excavating activities lessen runoff but facilitate soil erosion – A
818   simulation experiment, CATENA, 202, 105248, https://doi.org/10.1016/j.catena.2021.105248, 2021.

819 Choi, K., Arnhold, S., Huwe, B., and Reineking, B.: Daily Based Morgan–Morgan–Finney (DMMF)
820   Model: A Spatially Distributed Conceptual Soil Erosion Model to Simulate Complex Soil Surface
821   Configurations, Water, 9, 278, https://doi.org/10.3390/w9040278, 2017.

822 Cohen, S., Willgoose, G., Svoray, T., Hancock, G., and Sela, S.: The effects of sediment transport,
823   weathering, and aeolian mechanisms on soil evolution, J. Geophys. Res. Earth Surf., 120, 260–274,
824   https://doi.org/10.1002/2014JF003186, 2015.

825 Cohen, S., Willgoose, G., and Hancock, G.: The mARM3D spatially distributed soil evolution model:
826   Three-dimensional model framework and analysis of hillslope and landform responses, J. Geophys.
827   Res., 115, 191, https://doi.org/10.1029/2009JF001536, 2010.

828 Coombes, M. A.: Biogeomorphology: diverse, integrative and useful, Earth Surf. Process. Landforms,
829   41, 2296–2300, https://doi.org/10.1002/esp.4055, 2016.

830 Corenblit, D., Corbara, B., and Steiger, J.: Biogeomorphological eco-evolutionary feedback between life
831   and geomorphology: a theoretical framework using fossorial mammals, Die Naturwissenschaften,
832   108, 55, https://doi.org/10.1007/s00114-021-01760-y, 2021.

833 Debruyn, L. A.L. and Conacher, A. J.: The bioturbation activity of ants in agricultural and naturally
834   vegetated   habitats   in   semiarid   environments,   Soil   Res.,   32,   555,
835   https://doi.org/10.1071/SR9940555, 1994.

836 Devia, G. K., Ganasri, B. P., and Dwarakish, G. S.: A Review on Hydrological Models, Aquatic Procedia,
837   4, 1001–1007, https://doi.org/10.1016/j.aqpro.2015.02.126, 2015.

838 Durner, W., Iden, S. C., and Unold, G. von: The integral suspension pressure method (ISP) for precise
839   particle-size analysis by gravitational sedimentation, Water Resour. Res., 53, 33–48,
840   https://doi.org/10.1002/2016WR019830, 2017.

841 Eccard, J. A. and Herde, A.: Seasonal variation in the behaviour of a short-lived rodent, BMC ecology,
842   13, 43, https://doi.org/10.1186/1472-6785-13-43, 2013.

843 Ferro, L. I. and Barquez, R. M.: Species Richness of Nonvolant Small Mammals Along Elevational
844   Gradients in Northwestern Argentina, Biotropica, 41, 759–767, https://doi.org/10.1111/j.1744-
845   7429.2009.00522.x, 2009.

846 Foster, D. W.: BIOTURB: A FORTRAN program to simulate the effects of bioturbation on the vertical
847   distribution of sediment, Computers & Geosciences, 11, 39–54, https://doi.org/10.1016/0098-
848   3004(85)90037-8, 1985.

849 François, F., Poggiale, J.-C., Durbec, J.-P., and Stora, G.: A New Approach for the Modelling of
850   Sediment Reworking Induced by a Macrobenthic Community, Acta Biotheoretica, 45, 295–319,
851   https://doi.org/10.1023/A:1000636109604, 1997.

852 Gabet, E. J., Reichman, O. J., and Seabloom, E. W.: The Effects of Bioturbation on Soil Processes and
853   Sediment   Transport,   Annu.   Rev.   Earth   Planet.   Sci.,   31,   249–273,
854   https://doi.org/10.1146/annurev.earth.31.100901.141314, 2003.

855 Gray, H. J., Keen-Zebert, A., Furbish, D. J., Tucker, G. E., and Mahan, S. A.: Depth-dependent soil
856   mixing persists across climate zones, Proceedings of the National Academy of Sciences of the
857   United States of America, 117, 8750–8756, https://doi.org/10.1073/pnas.1914140117., 2020.

858 Grigusova, P., Larsen, A., Achilles, S., Brandl, R., del Río, C., Farwig, N., Kraus, D., Paulino, L., Pliscoff,
859   P., Übernickel, K., and Bendix, J.: Higher sediment redistribution rates related to burrowing animals
860   than previously assumed as revealed by time-of-flight-based monitoring, Earth Surf. Dynam., 10,
861   1273–1301, https://doi.org/10.5194/esurf-10-1273-2022, 2022.

862 Grigusova, P., Larsen, A., Achilles, S., Klug, A., Fischer, R., Kraus, D., Übernickel, K., Paulino, L.,
863   Pliscoff, P., Brandl, R., Farwig, N., and Bendix, J.: Area-Wide Prediction of Vertebrate and
864   Invertebrate Hole Density and Depth across a Climate Gradient in Chile Based on UAV and Machine
865   Learning, Drones, 5, 86, https://doi.org/10.3390/drones5030086, 2021.

866 Hakonson, T. E.: The Effects of Pocket Gopher Burrowing on Water Balance and Erosion from Landfill
867   Covers, J. environ. qual., 28, 659–665, https://doi.org/10.2134/jeq1999.00472425002800020033x,
868   1999.

869 Hall, K., Boelhouwers, J., and Driscoll, K.: Animals as Erosion Agents in the Alpine Zone: Some Data
870   and Observations from Canada, Lesotho, and Tibet, Arctic, Antarctic, and Alpine Research, 31, 436–
871   446, https://doi.org/10.1080/15230430.1999.12003328, 1999.

872 Hancock, G. and Lowry, J.: Quantifying the influence of rainfall, vegetation and animals on soil erosion
873   and hillslope connectivity in the monsoonal tropics of northern Australia, Earth Surf. Process.
874   Landforms, 46, 2110–2123, https://doi.org/10.1002/esp.5147, 2021.

875 Hazelhoff, L., van Hoof, P., Imeson, A. C., and Kwaad, F. J. P. M.: The exposure of forest soil to erosion
876   by earthworms, Earth Surf. Process. Landforms, 6, 235–250,
877   https://doi.org/10.1002/esp.3290060305, 1981.

878 Horn, B.K.P.: Hill shading and the reflectance map, Proc. IEEE, 69, 14–47,
879   https://doi.org/10.1109/PROC.1981.11918, 1981.

880 Imeson, A. C. and Kwaad, F. J. P. M.: Some Effects of Burrowing Animals on Slope Processes in the
881   Luxembourg Ardennes, Geografiska Annaler: Series A, Physical Geography, 58, 317–328,
882   https://doi.org/10.1080/04353676.1976.11879941, 1976.

883 Istanbulluoglu, E.: Vegetation-modulated landscape evolution: Effects of vegetation on landscape
884   processes, drainage density, and topography, J. Geophys. Res., 110, 11,
885   https://doi.org/10.1029/2004JF000249, 2005.

886 Jimenez, J. E., Feinsinger, P., and Jaksi, F. M.: Spatiotemporal Patterns of an Irruption and Decline of
887   Small Mammals in Northcentral Chile, Journal of Mammalogy, 73, 356–364,
888   https://doi.org/10.2307/1382070, 1992.

889 Jong, S. M. de, Paracchini, M. L., Bertolo, F., Folving, S., Megier, J., and Roo, A.P.J. de: Regional
890   assessment of soil erosion using the distributed model SEMMED and remotely sensed data,
891   CATENA, 37, 291–308, https://doi.org/10.1016/S0341-8162(99)00038-7, 1999.

892 Jumars, P. A., Nowell, A. R.M., and Self, R. F.L.: A simple model of flow—Sediment—Organism
893   interaction, Marine Geology, 42, 155–172, https://doi.org/10.1016/0025-3227(81)90162-6, 1981.

894 Katzman, E. A., Zaytseva, E. A., Feoktistova, N. Y., Tovpinetz, N. N., Bogomolov, P. L., Potashnikova,
895   E. V., and Surov, A. V.: Seasonal Changes in Burrowing of the Common Hamster (Cricetus cricetus
896   L., 1758) (Rodentia: Cricetidae) in the City, PJE, 17, 251–258, https://doi.org/10.18500/1684-7318-
897   2018-3-251-258, 2018.

898 Kinlaw, A. and Grasmueck, M.: Evidence for and geomorphologic consequences of a reptilian
899   ecosystem engineer: The burrowing cascade initiated by the Gopher Tortoise, Geomorphology, 157-
900   158, 108–121, https://doi.org/10.1016/j.geomorph.2011.06.030, 2012.

901 Kirols, H. S., Kevorkov, D., Uihlein, A., and Medraj, M.: The effect of initial surface roughness on water
902   droplet erosion behaviour, Wear, 342-343, 198–209, https://doi.org/10.1016/j.wear.2015.08.019,
903   2015.

904 Kraus, D., Brandl, R., Achilles, S., Bendix, J., Grigusova, P., Larsen, A., Pliscoff, P., Übernickel, K., and
905   Farwig, N.: Vegetation and vertebrate abundance as drivers of bioturbation patterns along a climate
906   gradient, PloS one, 17, e0264408, https://doi.org/10.1371/journal.pone.0264408, 2022.

907 Kügler, M., Hoffmann, T. O., Beer, A. R., Übernickel, K., Ehlers, T. A., Scherler, D., and Eichel, J.:
908   (LiDAR) 3D Point Clouds and Topographic Data from the Chilean Coastal Cordillera, 2022.

909 Lal, R.: Soil degradation by erosion, Land Degrad. Dev., 12, 519–539, https://doi.org/10.1002/ldr.472,
910   2001.

911 Larsen, A., Nardin, W., Lageweg, W. I., and Bätz, N.: Biogeomorphology, quo vadis? On processes,
912   time, and space in biogeomorphology, Earth Surf. Process. Landforms, 46, 12–23,
913   https://doi.org/10.1002/esp.5016, 2021.

914 Le Hir, P., Monbet, Y., and Orvain, F.: Sediment erodability in sediment transport modelling: Can we
915   account for biota effects?, Continental Shelf Research, 27, 1116–1142,
916   https://doi.org/10.1016/j.csr.2005.11.016, 2007.

917 Lehnert, L. W., Thies, B., Trachte, K., Achilles, S., Osses, P., Baumann, K., Schmidt, J., Samolov, E.,
918   Jung, P., Leinweber, P., Karsten, U., Büdel, B., and Bendix, J.: A Case Study on Fog/Low Stratus
919   Occurrence at Las Lomitas, Atacama Desert (Chile) as a Water Source for Biological Soil Crusts,
920   Aerosol Air Qual. Res., 18, 254-26, https://doi.org/10.4209/aaqr.2017.01.0021, 2018.

921 Li, G., Li, X., Li, J., Chen, W., Zhu, H., Zhao, J., and Hu, X.: Influences of Plateau Zokor Burrowing on
922   Soil Erosion and Nutrient Loss in Alpine Meadows in the Yellow River Source Zone of West China,
923   Water, 11, 2258, https://doi.org/10.3390/w11112258, 2019a.

924 Li, T. C., Shao, M. A., Jia, Y. H., Jia, X. X., Huang, L. M., and Gan, M.: Small-scale observation on the
925   effects of burrowing activities of ants on soil hydraulic processes, Eur J Soil Sci, 70, 236–244,
926   https://doi.org/10.1111/ejss.12748, 2019b.

927 Li, T., Shao, M.'a., Jia, Y., Jia, X., and Huang, L.: Small-scale observation on the effects of the burrowing
928   activities of mole crickets on soil erosion and hydrologic processes, Agriculture, Ecosystems &
929   Environment, 261, 136–143, https://doi.org/10.1016/j.agee.2018.04.010, 2018.

930 Li, Z. and Zhang, J.: Calculation of Field Manning's Roughness Coefficient, Agricultural Water
931   Management, 49, 153–161, https://doi.org/10.1016/S0378-3774(00)00139-6, 2001.

932 Lilhare, R., Garg, V., and Nikam, B. R.: Application of GIS-Coupled Modified MMF Model to Estimate
933   Sediment Yield on a Watershed Scale, J. Hydrol. Eng., 20, 745,
934   https://doi.org/10.1061/(ASCE)HE.1943-5584.0001063, 2015.

935 López-Vicente, M., Navas, A., and Machín, J.: Modelling soil detachment rates in rainfed agrosystems
936   in the south-central Pyrenees, Agricultural Water Management, 95, 1079–1089,
937   https://doi.org/10.1016/j.agwat.2008.04.004, 2008.

938 Malizia, A. I.: Population dynamics of the fossorial rodent Ctenomys talarum (Rodentia: Octodontidae),
939   Journal of Zoology, 244, 545–551, https://doi.org/10.1111/j.1469-7998.1998.tb00059.x, 1998.

940 Merritt, W. S., Letcher, R. A., and Jakeman, A. J.: A review of erosion and sediment transport models,
941   Environmental Modelling & Software, 18, 761–799, https://doi.org/10.1016/S1364-8152(03)00078-
942   1, 2003.

943 Meserve, P. L.: Trophic Relationships among Small Mammals in a Chilean Semiarid Thorn Scrub
944   Community, Journal of Mammalogy, 62, 304–314, https://doi.org/10.2307/1380707, 1981.

945 Meyer, H., Reudenbach, C., Hengl, T., Katurji, M., and Nauss, T.: Improving performance of spatio-
946   temporal machine learning models using forward feature selection and target-oriented validation,
947   Environmental Modelling & Software, 101, 1–9, https://doi.org/10.1016/j.envsoft.2017.12.001, 2018.

948 Meysman, F. J. R., Boudreau, B. P., and Middelburg, J. J.: Relations between local, nonlocal, discrete
949   and continuous models of bioturbation, J Mar Res, 61, 391–410,
950   https://doi.org/10.1357/002224003322201241, 2003.

951 Milstead, W. B., Meserve, P. L., Campanella, A., Previtali, M. A., Kelt, D. A., and Gutiérrez, J. R.: Spatial
952   Ecology of Small Mammals in North-central Chile: Role of Precipitation and Refuges, Journal of
953   Mammalogy, 88, 1532–1538, https://doi.org/10.1644/16-MAMM-A-407R.1, 2007.

954 Monteverde, M. J. and Piudo, L.: Activity Patterns of the Culpeo Fox (Lycalopex Culpaeus Magellanica
955   ) in a Non-Hunting Area of Northwestern Patagonia, Argentina, Mammal Study, 36, 119–125,
956   https://doi.org/10.3106/041.036.0301, 2011.

957 Morgan, R. P. C. and Duzant, J. H.: Modified MMF (Morgan–Morgan–Finney) model for evaluating
958   effects of crops and vegetation cover on soil erosion, Earth Surf. Process. Landforms, 33, 90–106,
959   https://doi.org/10.1002/esp.1530, 2008.

960 Morgan, R. P. C., Quinton, J. N., Smith, R. E., Govers, G., Poesen, J. W. A., Auerswald, K., Chisci, G.,
961   Torri, D., and Styczen, M. E.: The European Soil Erosion Model (EUROSEM): a dynamic approach
962   for predicting sediment transport from fields and small catchments, Earth Surf. Process. Landforms,
963   23, 527–544, https://doi.org/10.1002/(SICI)1096-9837(199806)23:6<527:AID-ESP868>3.0.CO;2-5,
964   1998.

965 Morgan, R.P.C.: A simple approach to soil loss prediction: a revised Morgan–Morgan–Finney model,
966   CATENA, 44, 305–322, https://doi.org/10.1016/S0341-8162(00)00171-5, 2001.

967 Morgan, R.P.C., Morgan, D.D.V., and Finney, H. J.: A predictive model for the assessment of soil erosion
968   risk, Journal of Agricultural Engineering Research, 30, 245–253, https://doi.org/10.1016/S0021-
969   8634(84)80025-6, 1984.

970 Nearing, M. A., Foster, G. R., Lane, L. J., and Finkner, S. C.: A Process-Based Soil Erosion Model for
971   USDA-Water Erosion Prediction Project Technology, Transactions of the ASAE, 32, 1587–1593,
972   https://doi.org/10.13031/2013.31195, 1989.

973 Nkem, J. N., Lobry de Bruyn, L. A., Grant, C. D., and Hulugalle, N. R.: The impact of ant bioturbation
974   and foraging activities on surrounding soil properties, Pedobiologia, 44, 609–621,
975   https://doi.org/10.1078/S0031-4056(04)70075-X, 2000.

976 Oeser, R. A., Stroncik, N., Moskwa, L.-M., Bernhard, N., Schaller, M., Canessa, R., van den Brink, L.,
977   Köster, M., Brucker, E., Stock, S., Fuentes, J. P., Godoy, R., Matus, F. J., Oses Pedraza, R., Osses
978   McIntyre, P., Paulino, L., Seguel, O., Bader, M. Y., Boy, J., Dippold, M. A., Ehlers, T. A., Kühn, P.,
979   Kuzyakov, Y., Leinweber, P., Scholten, T., Spielvogel, S., Spohn, M., Übernickel, K., Tielbörger, K.,
980   Wagner, D., and Blanckenburg, F. von: Chemistry and microbiology of the Critical Zone along a
981   steep climate and vegetation gradient in the Chilean Coastal Cordillera, CATENA, 170, 183–203,
982   https://doi.org/10.1016/j.catena.2018.06.002, 2018.

983 Pelletier, J. D., Barron-Gafford, G. A., Breshears, D. D., Brooks, P. D., Chorover, J., Durcik, M., Harman,
984   C. J., Huxman, T. E., Lohse, K. A., Lybrand, R., Meixner, T., McIntosh, J. C., Papuga, S. A.,
985   Rasmussen, C., Schaap, M., Swetnam, T. L., and Troch, P. A.: Coevolution of nonlinear trends in
986   vegetation, soils, and topography with elevation and slope aspect: A case study in the sky islands
987   of southern Arizona, J. Geophys. Res. Earth Surf., 118, 741–758, https://doi.org/10.1002/jgrf.20046,
988   2013.

989 Penman, H.: Natural evaporation from open water, hare soil and grass, Proceedings of the Royal Society
990   of London. Series A, Mathematical and physical sciences, 193, 120–145,
991   https://doi.org/10.1098/rspa.1948.0037, 1948.

992 Pollacco, J. A. P.: A generally applicable pedotransfer function that estimates field capacity and
993   permanent wilting point from soil texture and bulk density, Can. J. Soil. Sci., 88, 761–774,
994   https://doi.org/10.4141/CJSS07120, 2008.

995 Qin, Y., Yi, S., Ding, Y., Qin, Y., Zhang, W., Sun, Y., Hou, X., Yu, H., Meng, B., Zhang, H., Chen, J., and
996   Wang, Z.: Effects of plateau pikas' foraging and burrowing activities on vegetation biomass and soil
997   organic carbon of alpine grasslands, Plant Soil, 458, 201–216, https://doi.org/10.1007/s11104-020-
998   04489-1, 2021.

999 Reichman, O. J. and Seabloom, E. W.: The role of pocket gophers as subterranean ecosystem
1000   engineers, Trends in Ecology & Evolution, 17, 44–49, https://doi.org/10.1016/S0169-
1001   5347(01)02329-1, 2002.

1002 Renard, K., Foster, G., Weesies, G., and Porter, J.: RUSLE: The Revised Universal Soil Loss Equation,
1003   Journal of Soil Water Conservation, 30–33, 1991.

1004   Ridd, P. V.: Flow Through Animal Burrows in Mangrove Creeks, Estuarine, Coastal and Shelf Science,
1005   43, 617–625, https://doi.org/10.1006/ecss.1996.0091, 1996.

1006   Rodríguez-Caballero, E., Cantón, Y., Chamizo, S., Afana, A., and Solé-Benet, A.: Effects of biological
1007   soil crusts on surface roughness and implications for runoff and erosion, Geomorphology, 145-146,
1008   81–89, https://doi.org/10.1016/j.geomorph.2011.12.042, 2012.

1009   ROO, A. P. J. de, WESSELING, C. G., and RITSEMA, C. J.: LISEM: A SINGLE-EVENT PHYSICALLY
1010   BASED HYDROLOGICAL AND SOIL EROSION MODEL FOR DRAINAGE BASINS. I: THEORY,
1011   INPUT AND OUTPUT, Hydrol. Process., 10, 1107–1117, https://doi.org/10.1002/(SICI)1099-
1012   1085(199608)10:8<1107:AID-HYP415>3.0.CO;2-4, 1996.

1013   Rutin, J.: The burrowing activity of scorpions (Scorpio maurus palmatus) and their potential contribution
1014   to the erosion of Hamra soils in Karkur, central Israel, Geomorphology, 15, 159–168,
1015   https://doi.org/10.1016/0169-555X(95)00120-T, 1996.

1016   Schiffers, K., Teal, L. R., Travis, J. M. J., and Solan, M.: An open source simulation model for soil and
1017   sediment bioturbation, PloS one, 6, e28028, https://doi.org/10.1371/journal.pone.0028028, 2011.

1018   Shannon, C. E.: A Mathematical Theory of Communication, Bell System Technical Journal, 27, 379–
1019   423, https://doi.org/10.1002/j.1538-7305.1948.tb01338.x, 1948.

1020   Shull, D. H.: Transition-matrix model of bioturbation and radionuclide diagenesis, Limnol. Oceanogr.,
1021   46, 905–916, https://doi.org/10.4319/lo.2001.46.4.0905, 2001.

1022   Simonetti, J. A.: Microhabitat Use by Small Mammals in Central Chile, Oikos, 56, 309,
1023   https://doi.org/10.2307/3565615, 1989.

1024   Soetaert, K., Herman, P. M. J., Middelburg, J. J., Heip, C., deStigter, H. S., van Weering, T. C. E.,
1025   Epping, E., and Helder, W.: Modeling ^{210}Pb-derived mixing activity in ocean margin sediments:
1026   Diffusive   versus   nonlocal   mixing,   J   Mar   Res,   54,   1207–1227,
1027   https://doi.org/10.1357/0022240963213808, 1996.

1028   Taylor, A. R., Lenoir, L., Vegerfors, B., and Persson, T.: Ant and Earthworm Bioturbation in Cold-
1029   Temperate Ecosystems, Ecosystems, 22, 981–994, https://doi.org/10.1007/s10021-018-0317-2,
1030   2019.

1031   Temme, A. J.A.M. and Vanwalleghem, T.: LORICA – A new model for linking landscape and soil profile
1032   evolution: Development and sensitivity analysis, Computers & Geosciences, 90, 131–143,
1033   https://doi.org/10.1016/j.cageo.2015.08.004, 2016.

1034   Tews, J., Brose, U., Grimm, V., Tielbörger, K., Wichmann, M. C., Schwager, M., and Jeltsch, F.: Animal
1035   species diversity driven by habitat heterogeneity/diversity: the importance of keystone structures,
1036   Journal of Biogeography, 31, 79–92, https://doi.org/10.1046/j.0305-0270.2003.00994.x, 2004.

1037   Tomasella, J., Hodnett, M. G., and Rossato, L.: Pedotransfer Functions for the Estimation of Soil Water
1038   Retention   in   Brazilian   Soils,   Soil   Sci.   Soc.   Am.   J.,   64,   327–338,
1039   https://doi.org/10.2136/sssaj2000.641327x, 2000.

1040   Trauth, M. H.: TURBO: a dynamic-probabilistic simulation to study the effects of bioturbation on
1041   paleoceanographic   time   series,   Computers   &   Geosciences,   24,   433–441,
1042   https://doi.org/10.1016/S0098-3004(98)00019-3, 1998.

1043   Tucker, G. E. and Hancock, G. R.: Modelling landscape evolution, Earth Surf. Process. Landforms, 35,
1044   28–50, https://doi.org/10.1002/esp.1952, 2010.

1045   Übernickel, K., Pizarro-Araya, J., Bhagavathula, S., Paulino, L., and Ehlers, T. A.: Reviews and
1046   syntheses: Composition and characteristics of burrowing animals along a climate and ecological
1047   gradient, Chile, Biogeosciences, 18, 5573–5594, https://doi.org/10.5194/bg-18-5573-2021, 2021a.

1048   Übernickel, K., Ehlers, T. A., Paulino, L., and Fuentes Espoz, J.-P.: Time series of meteorological
1049   stations on an elevational gradient in National Park La Campana, Chile, 2021b.

Vanwalleghem, T., Stockmann, U., Minasny, B., and McBratney, A. B.: A quantitative model for integrating landscape evolution and soil formation, J. Geophys. Res. Earth Surf., 118, 331–347, https://doi.org/10.1029/2011JF002296, 2013.

Vieira, D.C.S., Prats, S. A., Nunes, J. P., Shakesby, R. A., Coelho, C.O.A., and Keizer, J. J.: Modelling runoff and erosion, and their mitigation, in burned Portuguese forest using the revised Morgan–Morgan–Finney model, Forest Ecology and Management, 314, 150–165, https://doi.org/10.1016/j.foreco.2013.12.006, 2014.

Vigiak, O., Okoba, B. O., Sterk, G., and Groenenberg, S.: Modelling catchment-scale erosion patterns in the East African Highlands, Earth Surf. Process. Landforms, 30, 183–196, https://doi.org/10.1002/esp.1174, 2005.

Voiculescu, M., Ianăș, A.-N., and Germain, D.: Exploring the impact of snow vole (Chionomys nivalis) burrowing activity in the Făgăraș Mountains, Southern Carpathians (Romania): Geomorphic characteristics and sediment budget, CATENA, 181, 104070, https://doi.org/10.1016/j.catena.2019.05.016, 2019.

Wang, B., Zheng, F., Römkens, M. J.M., and Darboux, F.: Soil erodibility for water erosion: A perspective and Chinese experiences, Geomorphology, 187, 1–10, https://doi.org/10.1016/j.geomorph.2013.01.018, 2013.

Wei, X., Li, S., Yang, P., and Cheng, H.: Soil erosion and vegetation succession in alpine Kobresia steppe meadow caused by plateau pika—A case study of Nagqu County, Tibet, Chin. Geograph.Sc., 17, 75–81, https://doi.org/10.1007/s11769-007-0075-0, 2007.

Welivitiya, W. D. D. P., Willgoose, G. R., and Hancock, G. R.: A coupled soilscape–landform evolution model: model formulation and initial results, Earth Surf. Dynam., 7, 591–607, https://doi.org/10.5194/esurf-7-591-2019, 2019.

Wheatcroft, R. A., Jumars, P. A., Smith, C. R., and Nowell, A. R. M.: A mechanistic view of the particulate biodiffusion coefficient: Step lengths, rest periods and transport directions, J Mar Res, 48, 177–207, https://doi.org/10.1357/002224090784984560, 1990.

Whitesides, C. J. and Butler, D. R.: Bioturbation by gophers and marmots and its effects on conifer germination, Earth Surf. Process. Landforms, 41, 2269–2281, https://doi.org/10.1002/esp.4046, 2016.

Wilkinson, M. T., Richards, P. J., and Humphreys, G. S.: Breaking ground: Pedological, geological, and ecological implications of soil bioturbation, Earth-Science Reviews, 97, 257–272, https://doi.org/10.1016/j.earscirev.2009.09.005, 2009.

Williams, J. R. (Ed.): Sediment-yield prediction with Universal Equation using runoff energy factor. In Present and prospective technology for predicting sediment yield and sources: Proceedings of the Sediment-Yield Workshop, ARS-S-40, United States Department of Agriculture (USDA), New Orleans, USA, 1975.

Wilson, M. F. J., O'Connell, B., Brown, C., Guinan, J. C., and Grehan, A. J.: Multiscale Terrain Analysis of Multibeam Bathymetry Data for Habitat Mapping on the Continental Slope, Marine Geodesy, 30, 3–35, https://doi.org/10.1080/01490410701295962, 2007.

Wischmeier, W. and Smith, D. D.: Predicting rainfall erosion losses - A guide to conservation planning, Agriculture Handbook, 1–58, 1978.

Wood, S. N.: Generalized Additive Models, Chapman and Hall/CRC, 2006.

Wösten, J.H.M. (Ed.): Soil Quality for Crop Production and Ecosystem Health, Developments in Soil Science, Elsevier, 1997.

Wu, C., Wu, H., Liu, D., Han, G., Zhao, P., and Kang, Y.: Crab bioturbation significantly alters sediment microbial composition and function in an intertidal marsh, Estuarine, Coastal and Shelf Science, 249, 107116, https://doi.org/10.1016/j.ecss.2020.107116, 2021.

1097   Yair, A.: Short and long term effects of bioturbation on soil erosion, water resources and soil
1098   development in an arid environment, Geomorphology, 13, 87–99, https://doi.org/10.1016/0169-
1099   555X(95)00025-Z, 1995.

1100   Yoo, K. and Mudd, S. M.: Toward process-based modeling of geochemical soil formation across diverse
1101   landforms: A   new   mathematical   framework,   Geoderma,   146,   248–260,
1102   https://doi.org/10.1016/j.geoderma.2008.05.029, 2008.

1103   Yoo, K., Amundson, R., Heimsath, A. M., and Dietrich, W. E.: Process-based model linking pocket
1104   gopher (Thomomys bottae) activity to sediment transport and soil thickness, J. Geophys. Res., 33,
1105   917, https://doi.org/10.1130/G21831.1, 2005.

1106   Yu, C., Zhang, J., Pang, X. P., Wang, Q., Zhou, Y. P., and Guo, Z. G.: Soil disturbance and disturbance
1107   intensity: Response of soil nutrient concentrations of alpine meadow to plateau pika bioturbation in
1108   the   Qinghai-Tibetan   Plateau,   China,   Geoderma,   307,   98–106,
1109   https://doi.org/10.1016/j.geoderma.2017.07.041, 2017.

1110   Zevenbergen, L. W. and Thorne, C. R.: Quantitative analysis of land surface topography, Earth Surf.
1111   Process. Landforms, 12, 47–56, https://doi.org/10.1002/esp.3290120107, 1987.

1112   Zhang, Q., Li, J., Hu, G., and Zhang, Z.: Bioturbation potential of a macrofaunal community in Bohai
1113   Bay,   northern   China,   Marine   pollution   bulletin,   140,   281–286,
1114   https://doi.org/10.1016/j.marpolbul.2019.01.063, 2019.

1115   Zhang, S., Fang, X., Zhang, J., Yin, F., Zhang, H., Wu, L., and Kitazawa, D.: The Effect of Bioturbation
1116   Activity of the Ark Clam Scapharca subcrenata on the Fluxes of Nutrient Exchange at the Sediment-
1117   Water Interface, J. Ocean Univ. China, 19, 232–240, https://doi.org/10.1007/s11802-020-4112-2,
1118   2020.

1119